The International Journal of Advanced Manufacturing Technology (2022) 121:6811–6836
https://doi.org/10.1007/s00170-022-09748-2

ORIGINAL ARTICLE

Investigating the 'techno-eco-efficiency' performance of pump impellers: metal 3D printing vs. CNC machining

Heshan Jayawardane[1] · Ian J. Davies[2] · J. R. Gamage[3] · Michele John[1] · Wahidul K. Biswas[1]

Received: 21 March 2022 / Accepted: 10 July 2022 / Published online: 23 July 2022

Abstract

The economic, environmental, and social impacts caused by the extensive resource consumption and harmful emissions from the metal manufacturing industry should be lowered through innovative sustainable manufacturing strategies. This study aims to investigate the techno-eco-efficiency performance of metal 3D-printed parts in comparison with CNC-machined parts to determine the technical, economic, and environmental performance as a decision support tool for selecting the most techno-eco-efficient manufacturing method. In this study, a novel metal extrusion 3D printing technology has been used to create a centrifugal semi-open pump impeller in 316L stainless steel material. The technical feasibility of the impellers has been determined by evaluating the geometry, build material, mechanics, morphology, and functional performance of the impellers. The eco-efficiency performance of technically feasible impellers was evaluated through environmental life cycle assessment, life cycle costing, and portfolio analysis. This eco-efficiency analysis helped ascertain the cost-competitiveness and environmentally friendliness of the 3D-printed impellers by comparing it with the conventional impellers. The findings reveal that the AM impeller is eco-efficient mainly due to lower normalised environmental impacts (54.6%) compared to the SM impeller. The functional parts made by metal extrusion 3D printing are technically feasible, cost-effective, and environmentally friendly compared to the SM counterparts.

Keywords Metal additive manufacturing · Sustainable manufacturing · Bound metal deposition · Metal extrusion · Life cycle assessment · Techno-eco-efficiency

Abbreviations

AM	Additive manufacturing
BMD	Bound metal deposition
CED	Cumulative energy demand
CMM	Coordinate measuring machine
CNC	Computer numerical control
DED	Directed energy deposition
EEA	Eco-efficiency assessment
EI	Environmental impact
ELCA	Environmental life cycle assessment
Eq.	Equivalent
FU	Functional unit
GDEI	Gross domestic environmental impact
GDP	Gross domestic product
GWP	Global warming potential
LCC	Life cycle costing
LCEI	Life cycle environmental impact
LCI	Life cycle inventory
Nei	Normalised environmental impact
NC	Normalised cost
NPV	Net present value
PBF	Powder bed fusion
PP	Portfolio position
UTS	Ultimate tensile stress

✉ Heshan Jayawardane
h.wijerath@postgrad.curtin.edu.au

Ian J. Davies
i.davies@curtin.edu.au

J. R. Gamage
gamagejr@uom.lk

Michele John
m.rosano@curtin.edu.au

Wahidul K. Biswas
w.biswas@curtin.edu.au

[1] Sustainable Engineering Group, School of Civil and Mechanical Engineering, Curtin University, Bentley, WA 6102, Australia

[2] School of Civil and Mechanical Engineering, Curtin University, Bentley, WA 6102, Australia

[3] Department of Mechanical Engineering, University of Moratuwa, Moratuwa, Sri Lanka

1 Introduction

The manufacturing value addition contributes 16.0% to global gross domestic product (GDP) [1] and accounts for significant portions of the total global energy consumption and environmental emissions. The main energy sources that support industrial energy consumption are oil (31.6%), coal (26.9%), and natural gas (22.8%) [2]. The manufacturing sector's energy use accounts for 24.2% of global greenhouse gas emissions, despite significant efforts to limit atmospheric emissions, solid waste, and effluents [3]. The manufacturing of metallic products is one of the main contributors to the environmental footprint of an industrial production system resulting mainly from the use of various metalworking processes and resource-intensive technologies [4]. The mining, material processing, manufacturing, usage, and disposal activities during the life cycle of metallic products cause significant emissions, waste, and resource depletion compared to non-metallic products [5]. Primary metal manufacturing alone accounts for 32.5% of the global coal energy consumption [2], and 16.9% of total energy consumption in Australia [6]. The industrial production of iron and steel accounts for 7.2% of global greenhouse gas emissions [3]. The extensive resource consumption and harmful emissions from the primary metal manufacturing industry should be lowered by applying innovative sustainable manufacturing strategies.

The manufacturing industry heavily relies on subtractive manufacturing (SM) technologies due to significant product quality gained by retaining the bulk material properties [7]. However, SM is resource inefficient as the material needs to be removed from the work blank using cutting tools to achieve the desired shape of the product [8]. Furthermore, these subtractive systems can only manufacture designs that cutting tools can reach, making them unable to produce complex metal parts [9]. The machining waste including machining lubricants, eventually end up in landfills, where they cause eco-toxicity [10]. The computer numerical control (CNC) machining approach using 3D model data has improved the efficiency of SM and minimised wastage while maintaining consistent product quality. Although the energy efficiency, cutting fluid control, and multi-axis operation of CNC machining have been constantly improved [11], waste generation cannot be totally eliminated.

Additive manufacturing (AM) or 3D printing is a cutting-edge manufacturing technique that can create functional components from polymers, ceramics, metals, composites, and biomaterials [12]. Metal AM methods include powder bed fusion (PBF), directed energy deposition (DED), binder jetting, metal material extrusion, and ultrasonic AM, depending on the manufacturing technology. The most common PBF AM technologies are selective laser melting (SLM) and electron beam melting (EBM), while the most common DED AM technologies are laser engineered net shaping (LENS), directed metal deposition (DMD), and electron beam additive manufacturing (EBAM) [13, 14]. Metal AM could be a promising alternative manufacturing option that may potentially address the aforementioned weaknesses associated with the use of SM for metallic components. Firstly, metal AM has the ability to produce complex, functional, high-value parts in a short lead time due to the elimination of tools, fixtures, and jigs used in SM [15]. Secondly, metal AM could reduce material wastage during the manufacturing process due to its additive nature [16]. Finally, metal AM could allow the fabrication of generative designs, simplifying the design stage costs [17]. However, AM possess several limitations such as limited material availability, high production time, high production cost, lower surface quality, residual stresses, and deformation of parts [18].

Metal AM methods such as SLM and EBM have the inherent drawbacks of high-energy consumption (31 kWh/kg for 316L stainless steel in SLM), high cost of metallic powder, toxicity of metallic powder, and its inability to make hollow parts due to the use of laser beams and electron beams as a primary energy source [19, 20]. Metal extrusion AM is a novel technology which addresses the limitations of conventional powder-based metal AM [21]. In several studies, metals have been mixed with polymers such as polylactic acid (PLA), resulting in higher technical properties than virgin polymers [22]. Furthermore, metals have also been mixed with ceramic clay to develop cermet materials. These materials could be extruded through piston or screw injectors for metal extrusion AM [17]. *Desktop Metal* and *Markforged* have commercialised this metal extrusion AM technology to produce functional metallic components for industrial, medical, aeronautical, and space applications [23, 24].

Desktop Metal's bound metal deposition (BMD) technology utilises conventional metal injection moulding principles to produce high-quality metal parts without incurring high production costs. This novel technology allows metal, bound within a ceramic binder to be extruded according to a 3D model. The obtained green part then needs to be debinded to remove the primary binder from the metal part through solvent decomposition. Then, the porous metal part is sintered in a furnace until the required metal density (96–99%) is obtained [23]. Post-processing methods such as polishing, sandblasting, heat treatment, and hot isostatic pressing have been used to improve surface properties, technical properties, and residual porosity of metal AM parts [25].

Since metal extrusion AM is relatively new, technical feasibility of the technology is still limited. Several studies,

however, have quantified the mechanical properties of metal 3D-printed parts from BMD technology [17, 26]. Thompson et al. [17] have stated that the density, dimensional measurement for shrinkage, and flexural strength of the 316L stainless steel specimens made by BMD is similar to rolled sheet metal bulk material. The findings also showed that BMD enables small-scale production of bespoke metal parts at a lower cost and reduced time, compared to conventional SM. Sadaf et al. [26] stated that 316L stainless steel specimens made by BMD exhibited a yield point of 250 MPa, a tensile strength of 520 MPa, and a Vickers microhardness of 285 HV, which is similar to the technical properties of conventional annealed steel. Jiang and Ning [25] have investigated the tensile and flexural fatigue properties of 316L stainless steel made through BMD, which has also shown feasible technical results compared to bulk material properties. All these studies have focused on the use of 316L stainless steel in metal AM and have evaluated its technical performance. However, it is also important to assess the performance of 3D-printed products during the use stage to investigate if AM has any effect on product's durability, as it could also change the economic and environmental impacts.

Stringent environmental regulations, increased environmental consciousness among the general public, and competitive markets have pushed manufacturers to consider cleaner production strategies to reduce the environmental footprint of manufacturing activities [7]. The environmental life cycle assessment (ELCA) has been the most effective tool for evaluating environmental impact [27]. Due to the novelty of BMD, there are no studies that evaluate the environmental impacts of BMD metal AM products. However, extensive studies have been conducted to evaluate the environmental performance of other metal AM technologies. Faludi et al. [19] have studied the environmental impact of aluminium in selective laser melting. The results showed that the cumulative energy demand during the manufacturing stage was the most dominant impact in the analysis while embodied energy per unit decreased with higher utilisation of the build envelope. Baumers et al. [20] have also studied the environmental impact of electron beam melting using the power consumption of metal AM under different build volume utilisation scenarios. Peng et al. [7] have studied the environmental impact of AM and SM under the indicators of global warming potential (GWP), acidification potential (AP), abiotic depletion potential (ADP), eutrophication potential (EP), and respiratory inorganics (RI) using the ELCA method. The results show that indicators of pure AM products are approximately twice that of SM products, mainly due to the high energy consumption and use of toxic metal powder.

The economic impact of manufacturing systems has predominantly been studied using life cycle costing (LCC) assessments [28, 29]. Studies have been conducted to evaluate the costs associated with BMD metal AM using LCC models. Watson et al. [30] stated that BMD technology has lowered the capital and operational costs of metal AM by 60–80% in comparison to PBF and DED. However, the study has not determined whether the benefit of cost reduction has occurred by reducing the technical performance of the 3D-printed products. Furthermore, there appear to have been no studies to date that determine the economic and environmental implications of the 3D printed products made from metal extrusion AM technology. Therefore, it warrants an investigation into whether functional metal AM parts can deliver reduced levels of environmental impact in a cost-competitive manner. In order to address this research question, a techno-eco-efficiency framework can be considered. Jayawardane et al. [31] developed this framework specifically for sustainable manufacturing research to evaluate the eco-efficiency performance of technically feasible parts through environmental life cycle assessment (ELCA), life cycle costing (LCC), and portfolio analyses. This study was conducted to evaluate the techno-eco-efficiency of polymer composite material made through fused filament fabrication. The same framework could be used to determine the technical feasibility and eco-efficiency performance of 316L stainless steel pump impellers through various assessments.

This study aims to investigate the techno-eco-efficiency performance of metal AM parts in comparison with metal SM parts to determine the technical, economic, and environmental performance of metal AM, as a decision support tool to select the most techno-eco-efficient manufacturing method for the selected part. The paper only focuses on the use of virgin material in a novel metal AM technology as the durability and mechanical performance of 3D-printed products are still unknown. Firstly, a technical feasibility assessment of AM specimens and parts has been conducted to investigate the influence of AM on durability of parts in the use stage of the given application. Following this, the study evaluated the economic and environmental impacts of metal AM parts compared to SM parts through a combination of ELCA and LCC for the eco-efficiency (EE) analysis to determine the techno-eco-efficient method for manufacturing the parts.

2 Materials and method

The techno-eco-efficiency framework (Fig. 1) developed by Jayawardane et al. [31] has been used in this study to evaluate the techno-eco-efficiency performance of manufactured parts. Firstly, the material feedstock will be used to 3D print the metallic components following the parametric configurations. Secondly, the technical feasibility of the 3D printed product will be evaluated by benchmarking

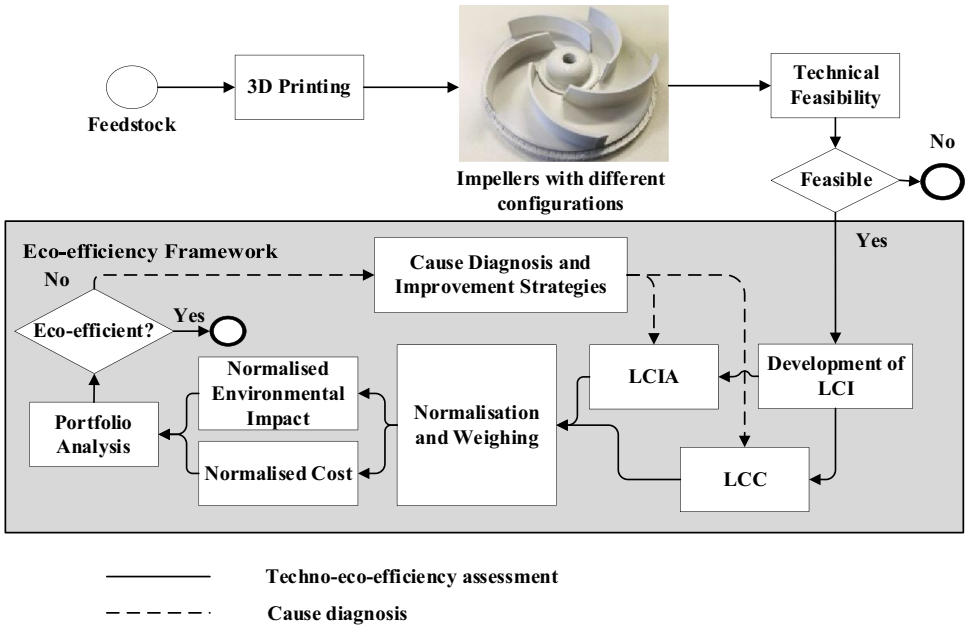

Fig. 1 Theoretical framework [31]

with CNC-machined counterparts, including their geometric properties, surface properties, mechanical properties, build material properties, and functional performance. The ELCA and LCC will be analysed and will be utilised in the eco-efficiency framework to determine the eco-efficiency performance of metal AM products and CNC-machined counterparts for comparative assessment.

Inputs (energy, material, utility, labour, and transport) and outputs (solid waste and emissions to air, water, and soil) during the life cycle stages, including material processing, manufacturing, and use of metal AM parts and SM parts were incorporated into the life cycle inventory (LCI). The SimaPro software has been used for the first stage of the ELCA, the life cycle impact assessment (LCIA) by converting the LCI into the relevant life cycle environmental impacts (LCEI) depending on the indicators selected through an expert survey. Alternatively, relevant cost values for corresponding inputs of LCI are used to estimate the LCC. The LCEI and LCC have been then normalised by dividing with relevant normalisation factors; LCEI with gross domestic environmental impact per inhabitant (GDEI/Inh) and LCC with gross domestic product per inhabitant (GDP/Inh). The normalised environmental impacts (NEI) are then weighted by multiplying them by the corresponding weighting factors. The final normalised values are used in the eco-efficiency portfolio analysis to determine the eco-efficiency of technically feasible parts through a comparative analysis. This framework developed by Jayawardane et al. [31] has been implemented to determine the techno-eco-efficiency of metal 3D printed parts.

2.1 Part selection

The same parts selection procedure adopted by Jayawardane et al. [31] has been followed in this research study. A centrifugal semi-open pump impeller has been selected as the most feasible product from a product portfolio (closed centrifugal pump impeller, semi-open centrifugal pump impeller, and spur gear). A feasibility score has been given to each product in terms of complexity, solid-to-envelope ratio, application, functionality, and availability of performance testing criteria. The semi-open centrifugal pump impeller has been selected with the highest feasibility score in this multi-criteria decision-making model [31]. The impeller is complex and comparatively difficult to manufacture by AM and SM methods. The impeller also has a high solid-to-envelope ratio, which makes it costly to manufacture using conventional SM methods. The impeller has also been scored on the availability of standard performance testing criteria for the functional application of a submersible wastewater pump (*Grundfos Unilift KP-250*) capable of pumping industrial and domestic effluents with particles up to 10 mm [32].

2.2 Manufacturing of pump impellers

A *Desktop Metal* Studio facility at Curtin University's John de Laeter Research Centre (JdLC) was utilised for metal additive manufacturing, while CNC machines (lathe, mill, drill) from the same university's manufacturing laboratory was used for conventional subtractive manufacturing. The 316L stainless steel material was selected from a *Desktop*

Metal material portfolio of 17–4 PH stainless steel, including 316L stainless steel, H13 tool steel, 4140 mild steel, and copper, because it is similar to the 304 stainless steel material used in the OEM pump impeller. The 316L stainless steel material has higher mechanical properties for a wide range of temperatures and possesses excellent corrosion resistance, thereby making it suitable for use in impellers under harsh environments. *Desktop Metal* 316L stainless steel material rods were used for metal 3D printing, and 316L stainless steel bulk material in billet form was used for CNC machining. Three impellers (AM1, AM2, AM3) were additive manufactured while three impellers (SM1, SM2, SM3) were subtractive manufactured.

2.2.1 Metal additive manufacturing

The centrifugal pump impeller (Fig. 2a and b) was 3D printed from 316L stainless steel by the *Desktop Metal* Studio 3D printer (Fig. 2c) using the BMD Technology.

The following configuration and parameters were used in 3D printing the pump impeller (Table 1). The 3D-printed 'green parts' were lightly cleaned with a brush to remove any scrap material and then debinded in the *Desktop Metal* debinder to remove the primary binder material. The debinded 'brown parts' were sintered to remove the residual binder and to solidify the final part.

2.2.2 Metal CNC machining

The impeller blade profiles for metal CNC machining were generated from the 3D model of the pump impeller using the *SolidWorks*® software. The benchmark pump impeller (Fig. 3a and b) was made from 316L stainless steel bulk material by subtractive manufacturing. The work blank for the impeller was a 316L stainless steel cylinder with a diameter of 100 mm. A *Leadwell* CNC lathe was used for turning the stainless steel work blank to the required diameter. The work blank was then machined using a *Leadwell V30* CNC milling machine (Fig. 3c) to manufacture the impeller blade profile. The coupling hole in the shape of the shaft profile of the pump was made using a *FANUC Robocut* wire electrode discharge machine (EDM). Finally, the impeller collar was CNC machined using the Leadwell V30 CNC milling machine separately and was spot welded to the impeller due to the difficulty in machining the impeller collar profile with the impeller vanes.

Table 1 Material and part configuration for 3D-printed impeller

Parameter	Configuration
Material	316L stainless steel
Material profile	Standard + profile
Extruder diameter	0.4 mm
Infill density (%)	100
Infill pattern	Solid (square cross-hath spacing)
Print speed	30.00 mm/s
Roof and floor thickness	1.80 mm
Roof and floor layers	24
Wall thickness	1.44 mm
Walls layers	3
Layer height	0.15 mm
Nozzle diameter	0.40 mm
Orientation/Raster angle	*XY*/0°
Printing temperature	175 °C
Build plate temperature	65 °C
Debinding temperature	250–350 °C
Sintering temperature	900–1250 °C
Sintering scale factor (x, y, z)	1.16

Table 2 shows the configuration and parameters of the machines used for the subtractive manufacturing of the benchmark pump impeller.

2.3 Technical feasibility assessment

Prior to the assessment of economic and environmental performance, technical performance should be evaluated. The following properties have been selected to be evaluated in the technical performance assessment.

2.3.1 Density

Porosity is an important consideration in metal 3D printing since it affects the mechanical response by acting as a null strength dispersed phase in a two-phase composite [26]. As a non-destructive method, product density has become

(a) (b) (c)

Fig. 2 3D printed pump impeller—front (**a**), 3D-printed pump impeller—rear (**b**), and *Desktop Metal* Studio in JDLC, Curtin University (**c**)

(a) (b) (c)

Fig. 3 SM pump impeller - front (**a**), SM pump impeller - rear (**b**), and *Leadwell V30* CNC milling machine (**c**)

an important measurement to determine the level of porosity of a component. Hence, the mean product density was determined following the ASTM D792/ISO 1183 standard method A. The mean density of the metal 3D printed impellers has been compared with the mean density of the CNC machined impellers in order to determine to test the effect of porosity in metal AM.

2.3.2 Surface roughness

The hydraulic and frictional losses within the pump can vary with the impeller's mean surface roughness (R_a) by changing the flow properties [31]. Therefore, a *Mitutoyo SJ-201* profilometer was used to measure the mean surface roughness of shrouds and vanes of the 3D-printed impellers (AM1, AM2, and AM3). The surface roughness of the AM impellers was benchmarked with the results of the SM impellers (SM1, SM2, and SM3).

2.3.3 Dimensional tolerance

The accurate measurement of dimensional tolerance of the pump impeller ensures fitting and clearance within the pump assembly. Peng et al. [7] state that the loose tolerance in the internal diameter of the impeller can cause improper fit and vibration between the impeller and pump shaft, resulting in impeller failure. Furthermore, tolerance of the outer diameter would affect the clearance between the impeller and pump housing. Therefore, dimensional measurements of the inner diameter (1), outer diameter (2), shroud thickness (3), and vane thickness (4) of the impeller (Fig. 4) were conducted using a *Sheffield Discovery II* coordinate measuring machine (CMM). The tolerances for OEM impeller were considered for comparison and benchmarking.

Table 2 Material and part configuration for CNC-machined impeller

Parameter	Configuration
Material	316L stainless steel
Machine 1	Leadwell CNC lathe
Machine 1 feed rate	96.60 m/min
Machine 2	Leadwell V30 vertical mill
Machine 2 feed rate	80.00 m/min
Machine 3	FANUC Robocut Wire EDM
Cutting tool	8.00 mm 3F EC high-speed steel
Depth of cut	0.20 mm
Width of cut	4.00 mm
Cutting fluid	ROCOL®

2.3.4 Geometric tolerance

The geometric tolerance measurement was conducted by 3D scanning the manufactured pump impellers using an *Artec Spyder* 3D scanner. The scanned model was aligned with the CAD model of the pump impeller by superimposition with specific alignment points at the vane surface. A distance map between the scanned model and the 3D CAD model was used to determine the degree of geometric deviation of the product features.

2.3.5 Tensile properties

The tensile properties which were deemed important for the mechanical performance of the impeller are ultimate tensile stress, percentage elongation, yield stress, and elastic modulus. Tensile strength indicates the material's response to withstand deformation due to tensile stresses. The impeller with higher tensile strength is more durable and offers longer service life due to higher fatigue properties. A uniaxial tensile test allows the measurement of these parameters. Six tensile test samples were manufactured and tested following the ASTM E8M standard to derive a stress–strain curve of the 3D printed 316L stainless steel material (AM1, AM2, AM3) and the 316L stainless steel bulk material (SM1, SM2, SM3) using a *Shimadzu Autograph* universal testing machine. The 3D-printed samples were printed in *XY*-orientation (along the build plate plane) with a 0° raster angle similar to the pump impellers. A load cell of 100 kN and a 5-mm/min crosshead speed was used in the tensile test to calculate the yield stress, ultimate tensile stress, percentage elongation, and elastic modulus along the *XY*-plane of the specimens.

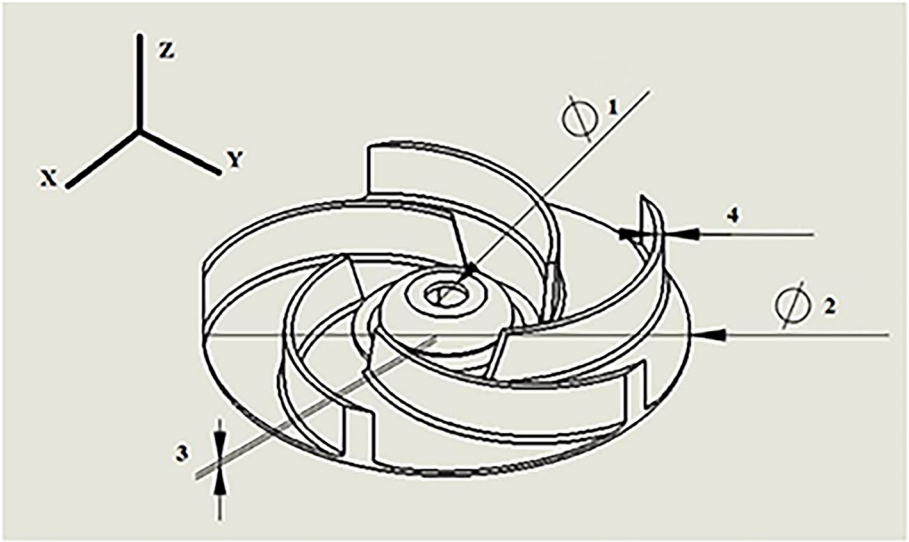

Fig. 4 Measured dimensions and orientation of the impeller

2.3.6 Fatigue properties

Fatigue properties such as fatigue strength and the number of cycles to failure are important in determining the service life of a component under cyclic loading conditions. A fatigue test determines the number of cycles to failure of a material at a specific stress level. The stress level at which the material withstands failure at a fatigue limit (10^6 cycles) is known as the fatigue strength. Materials failing at a higher number of fatigue cycles are more durable and possess an increased service life. The eco-efficiency performance could be potentially improved due to increased service life, which is an important consideration in the sustainability as it could help select the impeller with increased lifetime and resulting resource efficiency. A low cycle fatigue test was conducted with a reversed cycled rotating bending fatigue testing machine (Schenck-type) according to ISO 22407:2021. The fatigue test was displacement controlled with no deliberate stress concentrations. Nine test samples were tested for the number of cycles to failure at three different stress levels (90% of UTS, 80% of UTS, and 70% of UTS, which are above the material yield strength) for each manufacturing method.

The Basquin model equation (Eq. (1)) was used to model the *S–N* curves for the fatigue results of materials. The constants of the equation *(A, B)* were determined by substituting the applied cyclic tensile stress (*S*) and the number of cycles to failure (*N*) values for each stress level [33]. The fatigue life of an impeller was determined from the number of cycles to failure and pump speed (Eq. (2)).

$$S = A \times N^{B} \tag{1}$$

$$\text{Estimated fatigue life } (h) = N/\text{pump speed (cycles}/h) \tag{2}$$

2.3.7 Surface properties

The morphology of the 3D-printed surface and the fracture surface of the tensile specimens were used to explain the variations of technical properties of specimens. Pertuz et al. [33] stated that the defects and porosity within the specimen affect the technical performance. Therefore, the fracture morphology was observed using an Olympus BX51 light microscope. However, the voids and defects in specimens could not be quantified. The images were processed using the *ImageJ* software.

2.3.8 Hydraulic properties

The performance of the impeller in the functional application was determined by the ISO 9906 [34] standard for measuring hydraulic performance following the study of Jayawardane et al. [31]. The pump with different impellers was fitted to a pump test rig (Fig. 5). The water level at the suction point was used to calculate the static suction head (H_s) (Eq. (3)). The head at the discharge point ($H_{d,n}$) for each impeller (n) was measured by a pressure gauge. The pump head ($H_{\text{pump, }n}$) was calculated by the difference of pressure heads (Eq. (4)) assuming no head loss (h—suction height, ρ_w—density of water, g—acceleration due to gravity). A flowmeter and a stopwatch were used to calculate the flow rate.

$$H_s = h \times \rho_w \times g \tag{3}$$

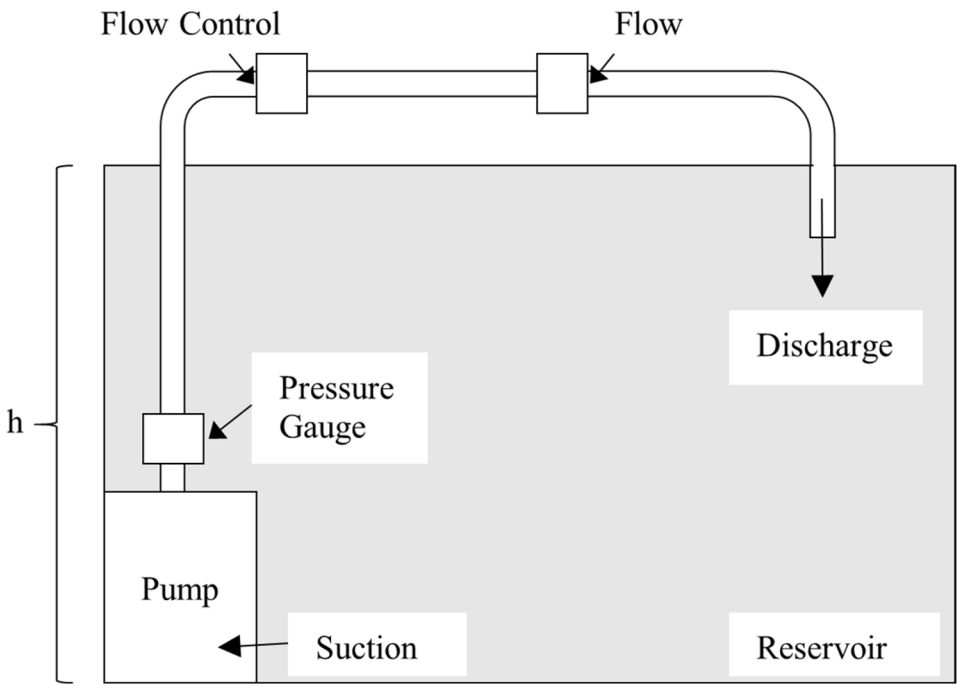

Fig. 5 Test rig for hydraulic performance [31]

$$H_{\text{pump},n} = H_{d,n} - H_s \tag{4}$$

The values of head (H) and flow rate (Q) obtained from the hydraulic performance test were used to draw the performance curves to determine the energy consumption of impellers manufactured by metal AM and CNC machining. The hydraulic performance of the original equipment manufacturer (OEM) pump impeller (304 stainless steel) was used to compare the hydraulic performance of AM and CNC manufactured impellers.

2.4 Environmental life cycle assessment (ELCA)

Only the metal AM impellers that were found technically feasible were considered for sustainability assessment. The environmental impacts were determined using an environmental life cycle assessment (ELCA) following the ISO 14040–44 standard [35]. The functional unit (FU), which is needed for conducting a mass balance to determine the inputs and outputs used during the life cycle of an impeller, was chosen as *'the delivery of fluid by an impeller over its service life*'. All life cycle stages from 'design to use' were included in the scope of ELCA, as shown in Fig. 6. The inputs and outputs of the life cycle stages, including energy, materials, utility, labour, waste, and emission, were used to develop an LCI. The finishing machining operations for the metal AM impeller have also been accounted in the manufacturing stage. The service life of each impeller was considered as the timeframe of the use stage. A similar LCI and scope has been used for the benchmark SM impeller. The end-of-life stage of the impeller, which could be either recovery or disposal of the pump impeller was not considered, as this study concerns the feasibility of the metal AM products.

The environmental impacts of each impeller have been calculated by the SimaPro LCA software [36]. The authors only used the environmental impact indicator values, which have been considered as relevant to the Australian manufacturing industry. Thirteen environmental impacts were selected through a consensus survey involving the Australian manufacturing experts [31]. Global warming potential (GWP), eutrophication, land use, water use, and cumulative energy demand (CED) were the only indicators that could be calculated using the Australian indicator method. Therefore, EPD (2013) V1.02 method was used to calculate acidification potential and abiotic depletion potential (ADP), ILCD 2011 Midpoint + V1.08 method was used to calculate photochemical smog and particulate matter, and eco-toxicity was calculated using the CML-IA baseline V3.03 method.

2.5 Life cycle costing (LCC)

The life cycle costing analysis was conducted to determine the economic impacts of metal AM and CNC machined impellers following the ELCA. Following the LCC framework of Jayawardane et al. [31], the goal, scope, system boundary and LCI of both ELCA and LCC were the same and their outputs have the same denominator, which allows the integration of ELCA and LCC outputs to determine the EE portfolios of alternative options for comparative

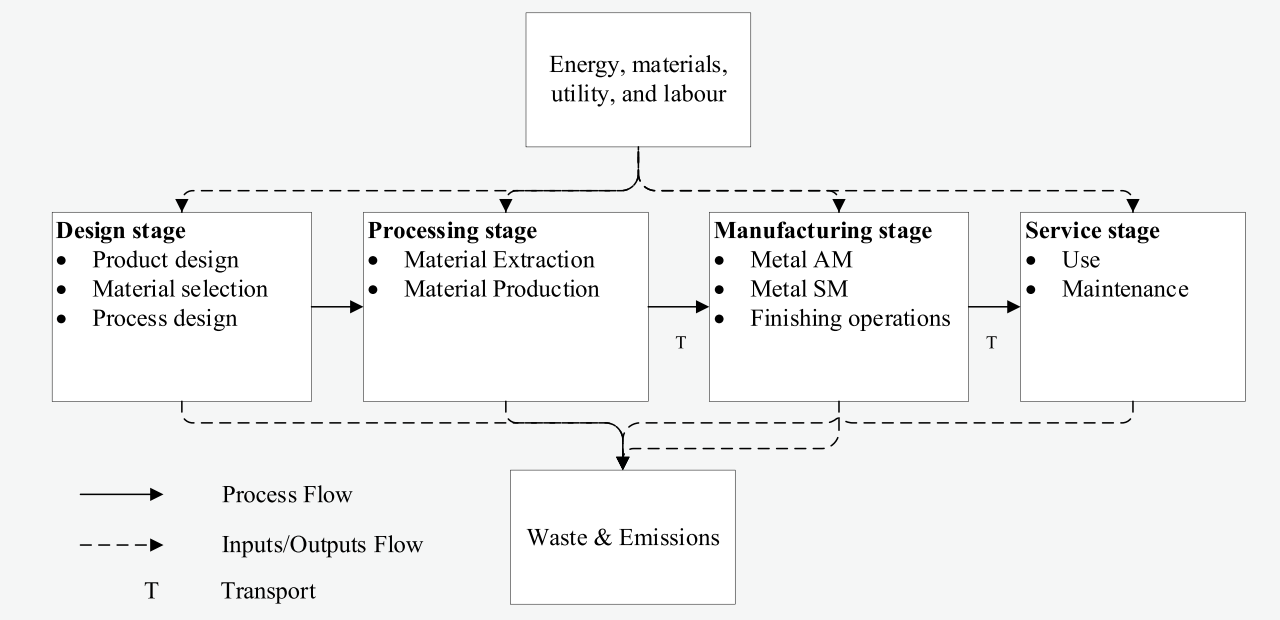

Fig. 6 The scope of ELCA [31]

purposes. The LCC was conducted to calculate the cost of *delivery of fluid during the service life of the impeller*. According to the AS/NZS 4536:1999 Australian/New Zealand Standard for life cycle costing—application guide [37], the LCC was calculated. The Microsoft Excel software was used to convert the LCI inputs to corresponding cost values obtained through a market survey. Only the labour costs which were included in the LCI were added to the cost items. The cost model was calculated in two steps: LCC of impeller production to calculate the unit cost of impellers, which was used as an input to the LCC of pumping operation. The end-of-life recovery or disposal costs were not incorporated in line with the scope of the ELCA. The LCC was performed in two steps:

Step 1: Capital costs, labour costs, energy costs, operations and maintenance costs, and transportation costs (Eq. (5)) from the design stage to the manufacturing stage were used to calculate the production cost of the impellers. The design stage costs include product design, process design, selection of material, and other utility costs [38]. The material processing costs included the raw material costs [23] and transportation costs from Massachusetts, USA to the metal 3D-printing facility in Perth, Australia [39]. The manufacturing stage overhead costs include the energy usage costs [40], equipment costs [23], and labour costs [41], which were apportioned to the manufacturing time for each impeller. A mass production of impellers was assumed for both the AM and SM over an equipment lifetime of 10 years (Eq. (5)). An inflation rate of 1.90% [42] and a discounting factor of 7% [43] were used in the LCC calculation. The sum of the present values (PV) of the costs incurred in stages from design to manufacturing was multiplied by the capital recovery factor (CRF) to obtain the annuitised cost (AC). The AC was then divided by the annual production output (PO) to obtain the life cycle cost of impeller production ($LCC_{Impeller,prod.}$) (Eq. (5)). The annuitised cost was converted to the price of an impeller (PI) using a profit margin (PM) of 35% [44] (Eq. (6)).

$$LCC_{Impeller,prod.} = (PV_{Capital} + PV_{Labour} + PV_{Energy} + PV_{O\&M}) \times CRF/PO \quad (5)$$

$$PI = LCC_{Impeller,prod.} \times (1 + PM) \quad (6)$$

Step 2: This determines the costs associated with the use of impellers in a commercial application. The calculated price of an impeller for pumping operation is considered as capital cost and the cost of electricity used for running this impeller is known as operating cost. $LCC_{pump\ usage}$ was therefore calculated by adding the PV of the price of an impeller (PI) to the operational costs during the service life (SL). The sum of PVs was multiplied by the CRF to obtain the AC, then divided by the impellers' service life (SL) [31] as presented in Eq. (7) in order to obtain the life cycle cost of pumping over the impeller SL ($LCC_{P,SL}$). The study did not consider maintenance costs of pump impellers as they were deemed negligible compared to other costs.

$$\mathrm{LCC}_{P,\mathrm{SL}} = (\mathrm{PV}_{\mathrm{PI}} + \mathrm{PV}_{\mathrm{energy}}) \times \mathrm{CRF}/\mathrm{SL} \quad (7)$$

2.6 Eco-efficiency assessment

The EE analysis compares the economic and environmental performance of 3D-printed impellers using the EE portfolio. The EE portfolio positions were calculated using both LCEI and LCC values of impellers [36]. In order for all LCEIs of impellers to convert to the same unit, they have been first normalised by dividing them by corresponding normalisation factors and then these normalised values were multiplied by corresponding weights. These impacts with the same units can then be compared. Each of these impacts is represented in terms of Australian inhabitants producing the same impact per year [45, 46]. The weighting factors were obtained from the results of the consensus survey, as shown in Table 21 in Appendix 1.

In order to obtain the normalised environmental impacts ($\mathrm{NEI}_{i,n}$), the LCEI values of the pump impeller type 'n' were divided (Eq. (8)) by the appropriate gross domestic environmental impact (GDEI_i/Inh). For each impact category, 'i', $\mathrm{NEI}_{i,n}$ was multiplied by their respective weights (W_i) (Eq. (9) in order to convert all impacts to the same unit so that all impact values could be combined to create a single value of overall environmental impact (EI_n) for an impeller 'n'. This EI_n is the number of Australian inhabitants who produced the same amount of environmental impact per year as the impeller of type 'n' [31].

$$\mathrm{NEI}_{i,n} = \frac{\mathrm{LCEI}_{i,n}}{\mathrm{GDEI}_i/Inh} \quad (8)$$

$$EI_n = \sum_{i=1}^{11} \mathrm{NEI}_{i,n} \times W_i \quad (9)$$

The normalised costs (NC_n) were obtained by dividing the life cycle cost (LCC_n) of a pump impeller 'n' with the relevant GDP/Inh (Eq. (10)). The GDP per capita of Australia in 2020 was taken as AUD 74,117 [47]. NC_n is the number of Australian inhabitants who produced the same amount of GDP as the cost of the impeller of type 'n' [31].

$$\mathrm{NC}_n = \frac{\mathrm{LCC}_n}{\mathrm{GDP/Inh}} \quad (10)$$

The environmental impact portfolio position of each impeller 'n' was obtained by dividing the normalised impact by the average value of EIs of all impellers. In contrast, the cost portfolio position was obtained by dividing the normalised cost of each impeller by the average value of NCs of all impellers (Eqs. (11) and (12)) [31].

$$\mathrm{PP}_{e,n} = \frac{\mathrm{EI}_n}{\sum \mathrm{EI}_n/j} \quad (11)$$

$$\mathrm{PP}_{c,n} = \frac{NC_n}{\sum \mathrm{NC}_n/j} \quad (12)$$

The environment to cost relevance ratio ($R_{E/C}$) was calculated as the ratio of mean EI and mean NC (Eq. (13)), which was used to determine the more influential parameter. Following Jayawardane et al. [31], the portfolio positions were revised by incorporating $R_{E/C}$ (Eqs. (14) and (15)). The revised portfolio positions ($\mathrm{PP'}_{e,n}$, $\mathrm{PP/'}_{c,n}$) were plotted in the EI_n vs. NC_n graph (Fig. 7).

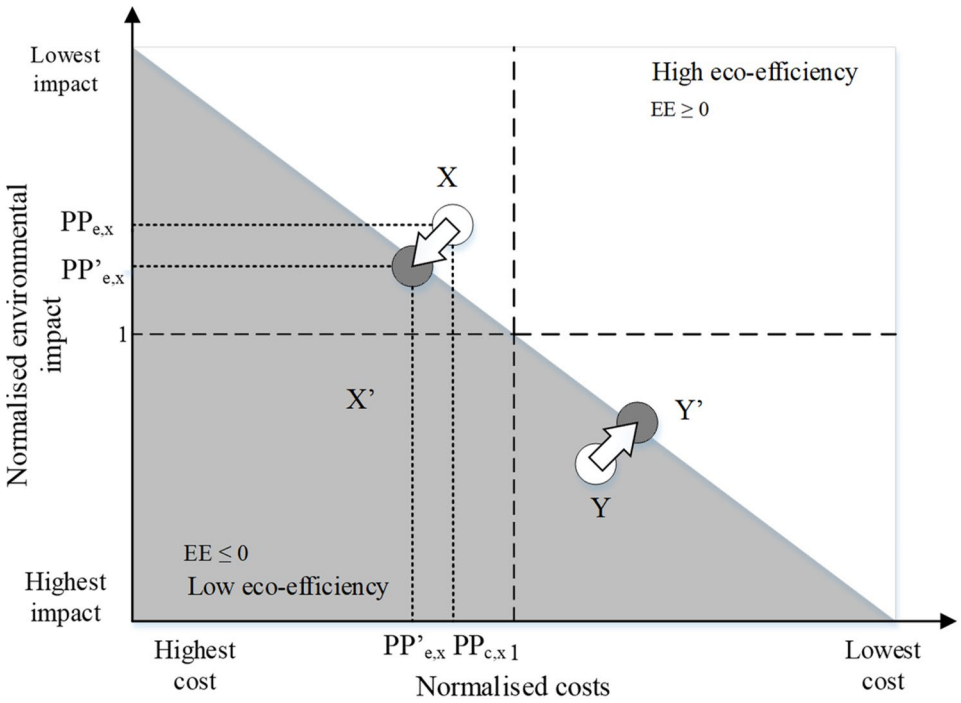

Fig. 7 EE portfolio and positions [31]

$$R_{E/C} = \frac{\sum EI_n/j}{\sum NC_n/j} \tag{13}$$

$$\mathrm{PP'_{e,n}} = \frac{\left[(\sum \mathrm{PP_{e,n}})/j + [\mathrm{PP_{e,n}} - ((\sum \mathrm{PP_{e,n}})/j)] \cdot \sqrt{(R_{E/C})}\right]}{(\sum \mathrm{PP_{e,n}})/\mathrm{j}} \tag{14}$$

$$\mathrm{PP'_{c,n}} = \frac{\left[(\sum \mathrm{PP_{c,n}})/j + [\mathrm{PP_{c,n}} - ((\sum \mathrm{PP_{c,n}})/j)] / \sqrt{(R_{E/C})}\right]}{(\sum \mathrm{PP_{c,n}})/\mathrm{j}} \tag{15}$$

The eco-efficiency portfolio positions were determined by following the eco-efficiency method by BASF [48]. In this EE portfolio, the most eco-efficient choice has the greatest perpendicular distance above the diagonal line. Due to the integration of the $R_{E/C}$, any changes in the cost or environmental impact of an impeller results in a change of EE portfolio positions of all impellers, as expressed by Eqs. (14) and (15). The impellers which are below the diagonal line were deemed environmentally inefficient, necessitating additional environmental and economic modifications to stay above or at least on the diagonal line.

3 Results and discussion

3.1 Technical feasibility assessment

3.1.1 Density

A mean product density of 7.78 g.cm^{-3} was obtained for the 3D-printed stainless steel impellers. In comparison, a mean product density of 7.94 g.cm^{-3} was obtained for the CNC-machined steel impellers in a density measurement using the specific gravity method at 22.1 °C. The metal 3D-printed sample indicates a relative density of 97.99% in the BMD 3D-printing process [23], resulting in a 316L stainless steel material with similar physical properties to bulk material properties. The presence of low internal voids, porosity, and defects could have led to the higher relative density in the metal AM sample. As a result, this could result in the sacrifice of tensile and fatigue outcomes slightly. Since the mean product density of typical metal injection moulded components (i.e., 7.6 g.cm^3) is lower than the mean product density of BMD parts, this reasonably confirms the technical feasibility aspects of the 3D printed impeller in terms of density.

3.1.2 Surface roughness

The surface roughness measurement showed the following results for the mean surface roughness (R_a) of the impeller shroud and the vanes, as presented in Table 3.

Table 3 Surface roughness measurement results

Impeller	Shroud R_a (μm)	Deviation (μm)	Vane R_a (μm)	Deviation (μm)
AM1	2.05	+1.25	3.98	+3.18
AM2	2.03	+1.23	3.36	+2.56
AM3	1.92	+1.12	3.60	+2.80
SM1	0.92	+0.12	0.45	−0.35
SM2	0.93	+0.13	0.47	−0.33
SM3	0.92	+0.12	0.47	−0.33
OEM	0.80		0.80	

The 3D-printed stainless steel impellers showed a slightly higher surface roughness than the CNC-machined stainless steel impellers in the shroud. This indicates an increase in surface roughness caused by the presence of print lines in the *XY*-direction for 3D printing. Furthermore, the surface roughness of the vanes was much higher than the surface roughness of the shroud, which indicates an increase in surface roughness due to the weaker layer stacking in the *Z*-direction for 3D printing. However, the surface roughness of the 3D-printed impellers was measured in the 'as printed' state and CNC-machined impellers were measured in an 'as machined' state before conducting any finishing CNC-machining operations. This was done to ensure that the surface roughness induced by additive and subtractive manufacturing processes could be directly compared.

Further finishing operations such as post polishing of pump impellers have not been incorporated in the selected pump impeller since reasonable surface roughness has been achieved for the low-cost application of the OEM pump for pumping wastewater. However, pump impellers and integrally bladed rotors in complex applications need further finishing operations such as abrasive flow machining [49, 50] to improve surface properties, which could yield better hydraulic performance. Post polishing could thus be considered in the future study.

3.1.3 Dimensional tolerance

The dimensional tolerances of the 3D-printed pump impeller and the CNC-machined pump impeller are presented in Tables 4 and 5. In 3D-printed impellers, the dimensions of the inner diameter did not meet the fitting tolerance with the pump shaft. CNC-milling machining operation was conducted to increase the inner diameter of the coupling hole of the impeller. Furthermore, the external diameters of the 3D-printed pump impellers were slightly higher than the OEM specification. However, this was allowable due to clearance between the impeller and the pump housing.

Higher dimensional tolerance values were observed in AM impeller due to the part shrinkage during the heat

Table 4 Dimensional measurements of pump impellers

Impeller	Inner diameter (mm)	External diameter (mm)	Vane thickness (mm)	Shroud thickness (mm)	Height (mm)
AM1	7.48	90.16	2.76	1.18	13.13
AM2	7.45	91.25	2.84	1.05	12.78
AM3	7.52	91.34	2.91	1.13	12.83
SM1	8.08	90.15	3.05	1.12	12.91
SM2	8.10	90.05	2.95	1.15	13.05
SM3	8.05	90.21	3.12	1.20	13.12
OEM	8.00	90.00	3.00	1.10	13.00

treatment process of the *Desktop Metal* Studio. Even though parts with a higher solid–cavity ratio have not exhibit high dimensional tolerances in other studies [26], parts with a lower solid–cavity ratio, such as a pump impeller, have shown high dimensional tolerances. The lower dimensional tolerances in shroud thickness and height measurement could be due to the lower shrinkage of parts in *Z*-direction in metal AM [14]. The CNC-machined pump impellers (SM1, SM2, and SM3) showed significantly better dimensional tolerances compared to the 3D-printed counterparts due to precision control of CNC equipment for machining bulk 316L stainless steel material.

3.1.4 Geometric tolerance

The geometric tolerance values were measured by a distance map between the superimposed scanned model and the 3D CAD model (Fig. 8), resulting in an absolute deviation of 0.113 mm and a root mean square deviation of 0.154 mm. The overall geometric measurements of the distance map indicate allowable tolerances as shown in the green region of the superimposed comparison image. Higher deviations were observed along the pump impeller vanes, but they were within the allowable range.

3.1.5 Tensile properties

The results show (Table 6, Fig. 9) slightly higher yield strength and slightly higher ultimate tensile strength values for 316L stainless steel bulk material compared to a stainless steel 3D-printed material. However, the 3D-printed specimens exhibited a more significant percentage elongation at the point of rupture, showing their superior ductile properties. The slightly lower tensile properties of AM specimens could be due to the lower relative density (97.99%) with the presence of internal voids, high porosity, and defects, which could lead to crack propagation. The tensile test results were similar to the results of 316L stainless steel material published by *Desktop Metal* (AM-DM) [23], Sadaf et al. [26], Gong et al. [51], and also similar to the tensile properties of 316L stainless steel specimen produced in metal injection moulding (MIM) [52].

Table 5 Dimensional tolerances

Parameter	AM (mm)	SM (mm)
Inner diameter	±0.50	±0.10
External diameter	±1.50	±0.25
Vane thickness	±0.25	±0.15
Shroud thickness	±0.10	±0.10
Height	±0.25	±0.15

3.1.6 Fatigue properties

The results of the fatigue properties were fit using the Basquin's model (Eq. (1)) for the finite fatigue life region of the material to obtain the Basquin's curve values (Table 7).

Figure 10 shows the logarithmic representation of the fatigue strength for 3D-printed (AM) and CNC-machined (SM) specimens. The results show that 3D-printed specimens possess similar fatigue life compared to that of CN-machined specimens when extrapolated with the Basquin's curve. This is due to the similar ultimate tensile strength values of both specimens contributing to similar fatigue strengths.

The results of the S–N curves of the fatigue test were used for the fatigue life calculation. The maximum pressure load acting on the impeller vanes at the steady-state operating conditions of the pump was set to 10 MPa [31, 53]. The fatigue strength was calculated as the stress value at 10^6 no. of cycles to failure. Table 8 shows the fatigue life calculations of the impellers. Jiang and Ning [25] have conducted a similar study investigating the fatigue strength of BMD 316L stainless steel, which showed a tensile fatigue strength of 100 MPa for 10^6 cycles. The results are also similar to the fatigue strength estimation of 316L stainless steel in SLM by Wang et al. [54].

The specimens exceeded the fatigue limit under cyclic loading. Therefore, it implies that the stainless steel impellers could last an infinite fatigue lifetime under standard steady-state operating conditions. However, this means that failure mechanisms, including foreign object impact damage, thermal damage, erosion, corrosion, and cavitation could determine the impeller service life. Hence, the estimated impeller service life for a submersible pump in standard operating conditions was determined as '1600 h' through the literature review. A pump usage of 4 h per day for 20 days a month (20 months) was estimated for the impellers for the use stage calculations [55, 56].

3.1.7 Surface properties

The morphology of the fracture surfaces of the tensile specimens was observed under the Olympus BX51

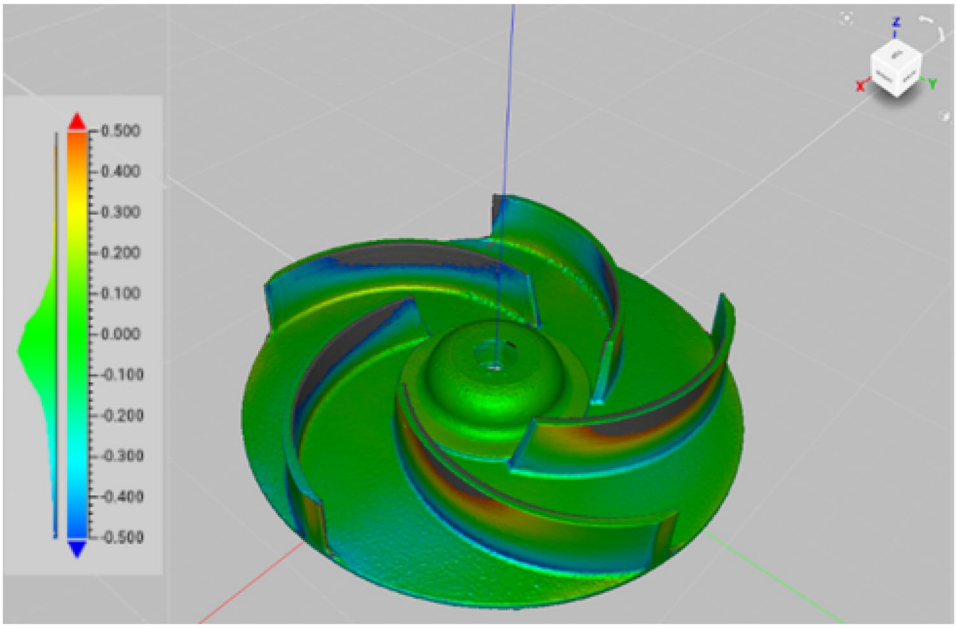

Fig. 8 Geometric tolerance distance map (scale is in mm)

light microscope. The metal 3D printed fracture surface showed a higher percentage of cavities, porosity, and defects (Fig. 11a). The surface topography examination of 3D-printed parts shows the presence of print layers (Fig. 11b–d). In contrast, the surface topography examination of CNC-machined parts (Fig. 11e) does not show any visible defects or porosity in the observed fracture surface of the specimen (Fig. 11f).

3.1.8 Hydraulic properties

The hydraulic performance of the pump impellers was tested using a recirculating pump test rig which resulted in the following data (Table 9) for 3D-printed impellers, CNC-machined impellers, and OEM impeller. The metal 3D-printed impellers and CNC-machined impellers have shown higher flow rates for similar pressure outputs, which indicates that the manufactured impellers are suitable in the application of sewage water pumping with small effluent particles.

Hydraulic performance curves (Fig. 12) were plotted using the data in Table 9. The results show that metal 3D-printed impellers and CNC-machined impellers outperform the OEM pump impeller in terms of hydraulic performance. This could be due to the weight of 304 stainless steel material used in the OEM pump impeller, which is higher than that of 316L stainless steel material used in metal 3D printing and CNC machining. The effect of higher surface roughness of the metal 3D-printed impeller and CNC machined impeller lowering the impeller performance could have been offset by the difference in weight of the impeller changing the flow curve.

3.1.9 Overall technical performance

The 3D-printed 316L stainless steel pump impeller shows similar properties compared to the benchmark of the CNC machined 316L stainless steel pump impeller. Table 10 presents the summary of the overall technical performance of pump impellers.

The surface roughness of the additive manufactured pump impeller is comparatively higher than that of the CNC machined pump impeller. The surface roughness of the impeller vanes is higher in the AM impeller due to non-uniform surface texture in the *Z*-direction caused by print

Table 6 Tensile test results

Specimen	Yield strength (MPa)	Ultimate tensile strength (MPa)	Elastic modulus (GPa)	Percentage elongation at break (%)
SM1	206.48	509.80	196.43	48.85
SM2	204.60	503.88	185.48	48.83
SM3	203.74	501.48	195.40	44.91
AM1	162.15	463.35	186.01	50.69
AM2	164.35	469.88	198.79	52.85
AM3	169.51	474.59	188.38	49.94
AM-DM	165.00	464.00	152.00	51.00
MIM	175.00	517.00	190.00	50.00

Table 7 Basquin's model values for specimens

	AM	SM
A	13,415.29	9323.95
B	−0.3188	−0.2776

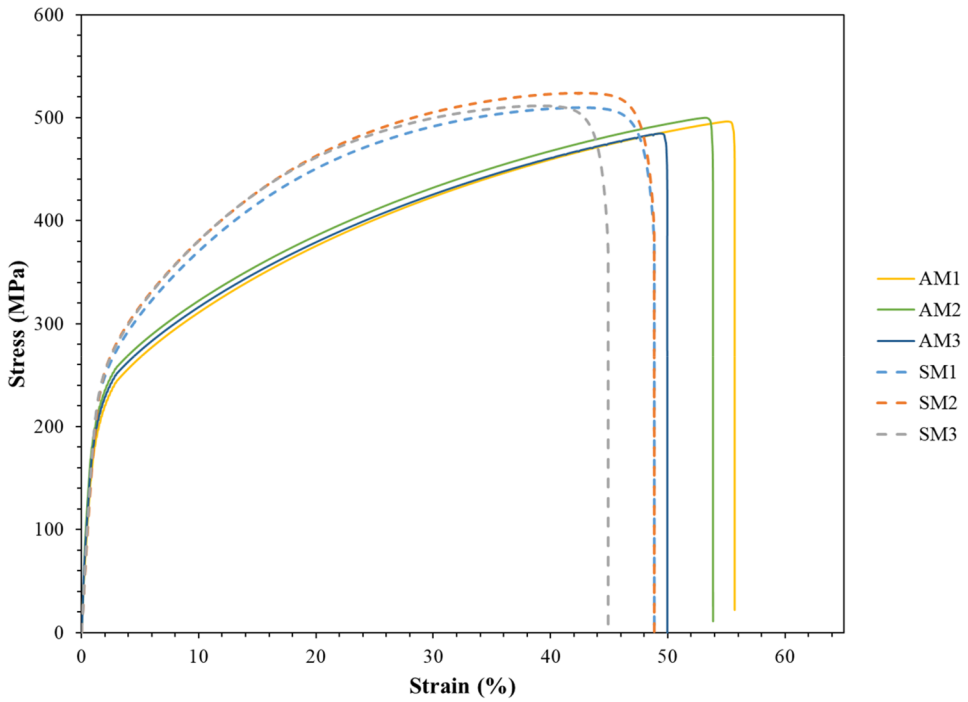

Fig. 9 Stress vs. strain curves for stainless specimens made by AM and SM methods

layers. In the SM impeller, the surface roughness of the shroud is higher due to surface texture from residual cuts from the end milling cutting tool.

The AM specimen has shown a part density of 97.8%, similar to conventional bulk material density. This shows that the sintering process has successfully eliminated the voids of the material, solidifying the 3D-printed material. The tensile strength of the AM material is very close (92.8%) to the tensile strength of the bulk material at an acceptable level, which is similar to the results of Sadaf et al. [26] using metal extrusion AM with 316L stainless steel material. The fatigue strength has slightly reduced (81.6%) due to the AM material having slightly lower tensile strength than the SM material, which was also found in the case of Jiang and Ning [25]. Interestingly, the hydraulic performance of the metal AM impeller was found to be higher than that of the OEM

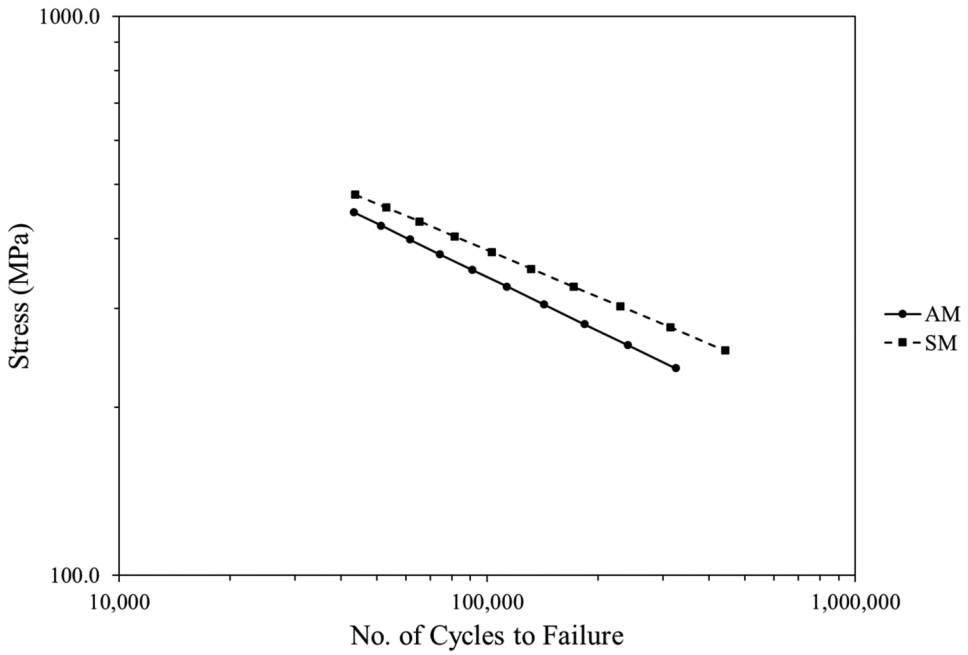

Fig. 10 Basquin's model curve for stress vs. no. of cycles to failure

Table 8 Predicted fatigue life of impellers at a stress of 10 MPa

Configuration (n)	Fatigue strength (MPa) @10^6 cycles	No. of cycles to failure @10 MPa	Fatigue lifetime-estimate (h) @10 MPa
SM	201.37	4.98E + 10	2.863E + 05
AM	163.98	6.46E + 09	3.715E + 04
BDM [25]	100	-	-
SLM [54]	200	-	-

impeller. Hence, the overall technical feasibility assessment suggests that a metal 3D printed pump impeller is reasonably technically feasible for the pumping industrial and domestic effluents with particles up to 10 mm.

3.2 Environmental life cycle assessment

Since AM and SM pump impellers were deemed technically feasible through the technical feasibility assessment, they were considered for the environmental life cycle assessment to determine the environmental impact of technically feasible impellers. The environmental impact indicators presented in Table 21 in Appendix 1 has been used in this assessment. The following production plan (Table 11) has been assumed to continue for the useful life of the manufacturing equipment.

The LCI of the pump impellers is presented in Table 12. The 3D printer has a comparatively higher material footprint than the CNC machine due to the combination of equipment (3D printer, debinder, and sintering furnace) needed for the complete metal extrusion process. Furthermore, the manufacturing stage energy consumption of the 3D-printed impeller has also increased due to the energy-intensive final sintering process (84%).

The following LCEI values were obtained for different impellers, as presented in Table 13. The metal 3D-printed impellers (AM) have shown higher LCEI values for environmental indicators such as GWP, europhication, land use, water use, ADP, acidification, particulate matter, and photochemical smog, which is similar to the results of Peng et al. [7]. However, CNC machined impellers (SM) have shown higher LCEI values for human toxicity (148%), freshwater eco-toxicity (304%), marine eco-toxicity (104%), and terrestrial eco-toxicity (39%). These values are consistent with the findings of Ingarao et al. [8]. The subtractive manufacturing process generates large amounts of metallic waste combined with cutting fluids, which could cause eco-toxicity of the land, freshwater bodies, and marine water bodies, and eventually cause human toxicity. After evaluating the environmental impacts, the economic impacts should be determined for further analysis in eco-efficiency assessment.

3.3 Life cycle costs

The life cycle costs have been determined for material processing, manufacturing, and usage stages. Table 14 presents the cost information input of the metal 3D printer (printer, debinder, sinter) and the CNC machine (lathe machine, milling machine) for the LCI data. These costs were then incorporated to determine the present values (PVs) of the material processing stage and manufacturing stages of the impellers (see Table 22 in Appendix 2).

The PVs of the material processing and manufacturing stages were used to calculate the PV of production costs according to the production plan. Table 15 presents the calculation of the prices of the impellers (PI) based on the production costs, annuities, and profit margin. A capital recovery factor (CRF) of 0.102 was used to convert the $PV_{total,\ prod}$ into annuities. The CRF was determined by the equipment's number of years of operation (10 years) and the discounting factor (7%). The annuities were then divided by the production output to obtain the $LCC_{impeller,\ prod}$, which is then converted to the price of the impeller after incorporating a profit margin of 35%.

The price of 3D-printed impellers and conventionally manufactured impellers were incorporated into the life cycle cost calculation as the capital cost. The energy consumption in pump operations was considered as the only operation and maintenance cost of the pump. Service costs and replacement costs of the pump were not considered since similar costs were incurred in both scenarios, and they cancel each other out. These LCC values were used to calculate the present value of the pump usage costs, as shown in Table 16. Firstly, the amount of energy consumed to pump water by each AM impeller and SM impeller was calculated while maintaining a fixed pressure head of 35 kPa. An impeller life of 1600 h or 20 months were estimated for both the AM and SM impellers, as per the fatigue life estimations in the previous technical feasibility assessment. A pump usage scenario of 4 h per day for 20 working days per month was assumed to calculate the pump's energy consumption (see "Sect. 3.1.7").

The results show that the AM impeller has a 2.1% higher cumulative electricity consumption than the SM impeller. This could be due to the lower hydraulic efficiency of the AM impeller ($\eta = 74\%$) compared to the SM impeller ($\eta = 78\%$). Furthermore, the capital cost of the AM impeller, which is 90.5% higher than the capital cost of the SM impeller, has resulted in a higher $PV_{total,p}$ for the AM impeller.

Table 17 presents the total life cycle cost of each impeller during the service life. The results show that the cost of pumping using a metal 3D-printed impeller is significantly more expensive than that for a CNC machined impeller. The equipment cost of metal 3D printing is approximately 4.25

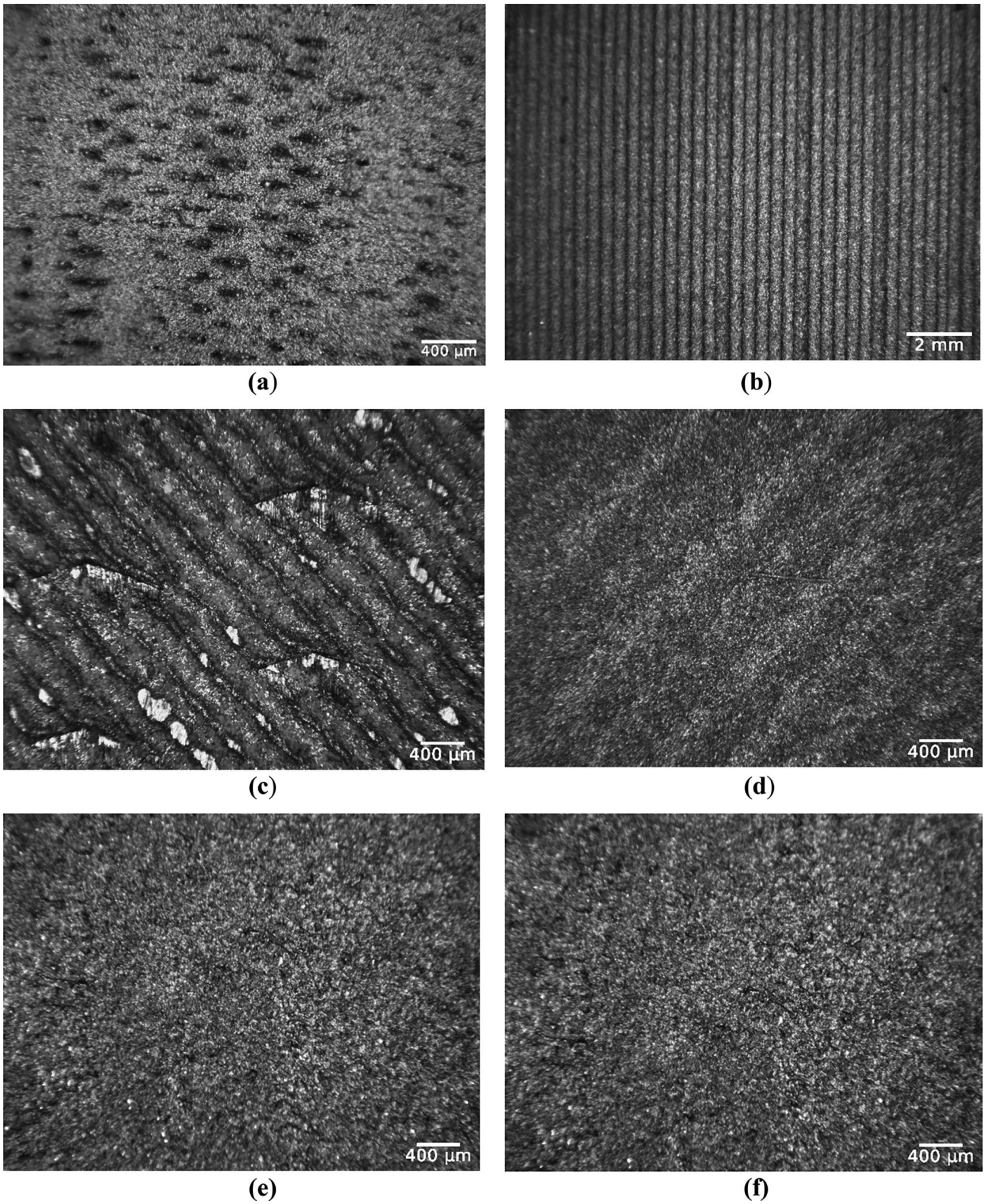

Fig. 11 Metal AM surface (**a**, **b**, **c**, **d**) and metal SM surface (**e**, **f**)

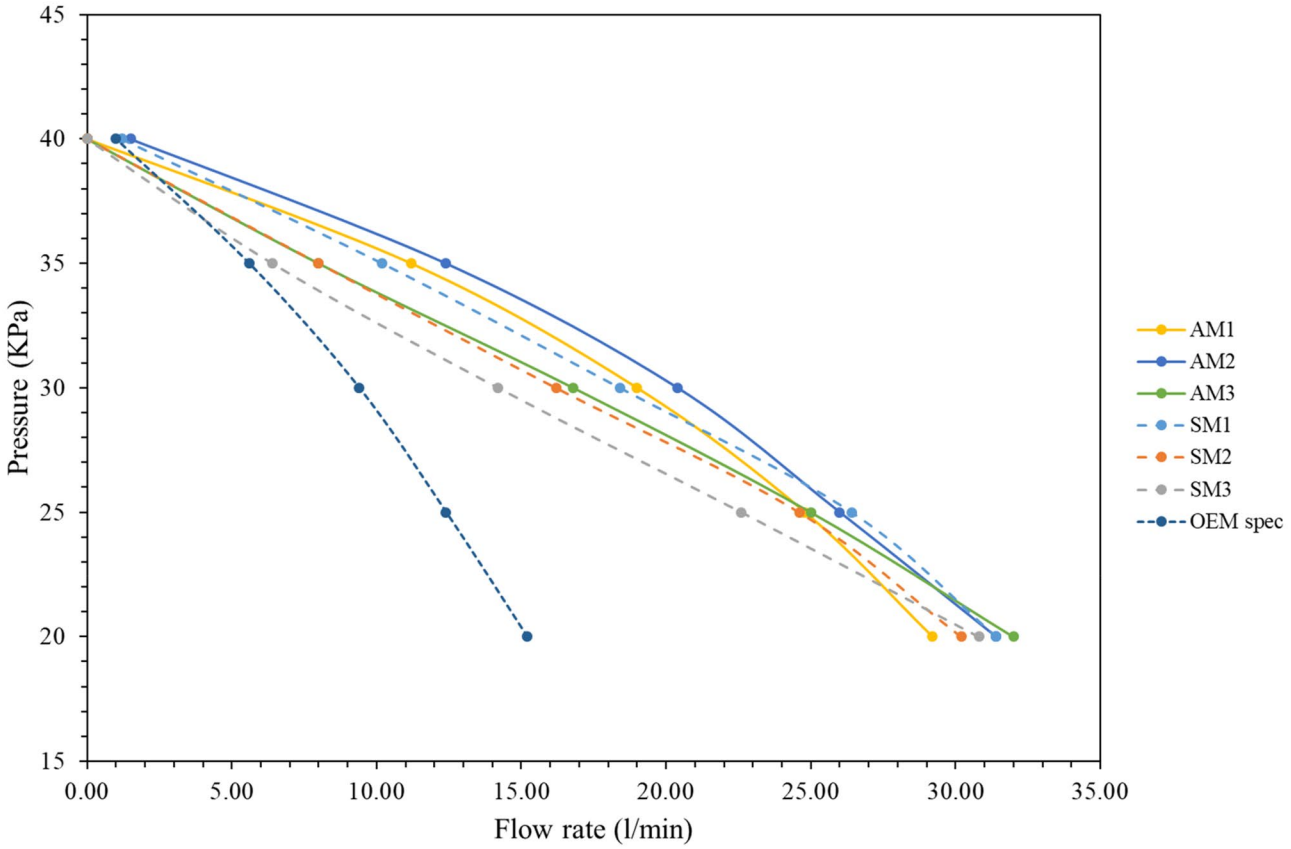

Fig. 12 Hydraulic performance curves

times higher than the equipment cost of CNC machining, which has resulted in very high capital costs. The novelty of the metal 3D-printing technology has resulted in high costs, which is similar to the cost results of Thompson et al. [17]. The equipment costs could reduce in the future with the widespread adoption of metal 3D-printing technology similar to the adoption of fused deposition modelling of thermoplastics [5]. However, due to the additive nature of metal 3D-printing technology, material wastage has been minimised. This is reflected in the production costs of the AM impeller, which is one third lower than the CNC machined impeller. Due to the high solid-to-envelope ratio of the semi-open pump impeller, a large amount of material needs to be removed in CNC machining, resulting in high material costs.

The overall $LCC_{P,\,SL}$ cost of AM impeller is 1.78 times higher than the SM impeller. Life cycle costing warrants further investigation with the integration of environmental

Table 9 Hydraulic performance data

		Pressure Output (kPa)				
	Impellers	20	25	30	35	40
$\dot{Q}$ (l/min)	SM1	31.40	26.40	18.40	10.20	1.20
	SM2	30.20	24.60	16.20	8.00	0.00
	SM3	30.80	22.60	14.20	6.40	0.00
	AM1	29.20	24.80	19.00	11.20	0.00
	AM2	31.40	26.00	20.40	12.40	1.50
	AM3	32.00	25.00	16.80	8.00	0.00
	OEM	15.20	12.40	9.40	5.60	1.00

impacts per dollar invested in the manufacturing process. Hence, an eco-efficiency assessment has been conducted to determine the eco-efficiency of metal 3D-printed impellers (AM) and CNC-machined impellers (SM).

3.4 Eco-efficiency Assessment

Since the metal 3D-printed impeller demonstrated about the same level of performance as the CNC-machined impeller, their eco-efficiency assessment could be conducted using ELCA and LCC results. Table 18 presents the normalised environmental impacts of AM and SM impellers after weighting and normalising to allow comparison between the two processes. The results show that NEI for an AM impeller was 55% lower than the SM impeller. When considering individual environmental impact indicators in Table 18, eco-toxicity was found to be the most significant indicator (49% of AM and 76% of SM) contributing to the total environmental impact with the highest contribution from the marine eco-toxicity (36.69% in AM and 67.37% in SM). This could be due to the use of toxic metals in the manufacturing stage, including aluminium, steel, copper, polycarbonates, and other plastics used in the production of manufacturing equipment (Table 12). The 316L stainless steel material used as the feedstock for AM and SM could end up in landfill or aquatic environments as manufacturing stage waste or as end-of-life products.

The next significant impact for metal 3D printing is the cumulative energy demand, which accounts for 15.95% of the AM total environmental impact. The AM energy demand is higher due to higher energy consumption in the manufacturing stage, which accounts for 76.2% of the energy consumption. The LCI values show that the metal sintering process is the most energy-intensive process in metal 3D printing, accounting for 84% of the total energy consumption. The printing process accounts for 5% of the CED, while the debinding process accounts for 10% of the CED. The GWP (10.46%) and photochemical smog (10.65%) are significant contributors to the total environmental impact of the metal 3D-printed products. The manufacturing stage of metal 3D-printing significantly contributes to the GWP (76.3%) and photochemical smog (75.6%).

The subtractive manufactured impeller exhibits a higher environmental impact, significantly contributed by the marine eco-toxicity. In order to obtain the shape of the semi-open impeller, a large amount of feedstock material needs to be removed from the work blank due to the lower solid-to-envelope ratio. This lower material efficiency of the subtractive manufacturing process produces metallic waste combined with coolant fluid, resulting in the release of metallic ions such as chromium or nickel. These metals are constituents of 316L stainless steel (composition: carbon 0.03%, chromium 16–18%, nickel 10–14%, manganese 2%, and molybdenum 2–3%) and could cause significant toxic effects [57]. These significant impact values are identified as hotspots in the ELCA. The normalised environmental impact values not only depend on the LCI inputs used in the product life cycle but also on the weighting factors determined by the consensus survey responses, which indicates GWP as the most significant (11.44%) followed by CED (11.44%). In comparison, land use is the least significant indicator (8.83%) out of the selected environmental impact indicators.

W_i weights, *EI* environmental impact, *TC* total contribution, *MPC* material processing stage contribution, *MfgC* manufacturing stage contribution; *UseC* use stage contribution, *GWP* global warming potential, *ADP* abiotic depletion potential, *CED* cumulative energy demand

Table 19 presents the overall normalised costs and normalised environmental impacts of the AM and SM impellers. These values were calculated according to Eqs. (8)–(10). The LCC values were normalised by dividing with the Australian GDP/Inh value of AUD 70,396.68 as of 2020.

The results show that the metal 3D-printing process could reduce the normalised environmental impact of conventional subtractive manufacturing by 54.6% lower than the conventional process. The substantial reduction of environmental impacts, such as marine eco-toxicity, in metal 3D printing, is reflected in this overall reduction of normalised environmental impact. However, the normalised cost of the metal 3D-printing process has increased the NCn by 43.8% higher than the conventional subtractive manufacturing process. This result infers that the capital costs of metal 3D printing should be reduced, which is expected to become possible by economies of scale after the widespread adoption of the technology. Integration of these values is needed to determine the environmental impact per dollar invested in this technology by conducting an eco-efficiency assessment.

The normalised environmental impacts and normalised costs have been used to determine the initial eco-efficiency portfolio positions. The $R_{E/C}$ value of 0.973 was obtained from Eq. (13), which shows that environmental impacts are almost as influential as the costs. The portfolio positions as presented in Table 20 were calculated from the Eqs. (13)–(15). Moreover, these portfolio positions were plotted on the graph of normalised environmental impact vs normalised cost, as shown in Fig. 13.

The results of the eco-efficiency portfolio show that the metal 3D-printed impeller has a portfolio position above the diagonal, whereas the CNC machined impeller has a portfolio position below the diagonal. This infers that the metal 3D printed pump impeller is eco-efficient whilst the CNC machined pump impeller is not eco-efficient. Compared to the CNC-machined impeller, the metal 3D printed impeller has attained eco-efficiency due to having a significantly lower normalised environmental impact (54.6%) than the former. The lower normalised

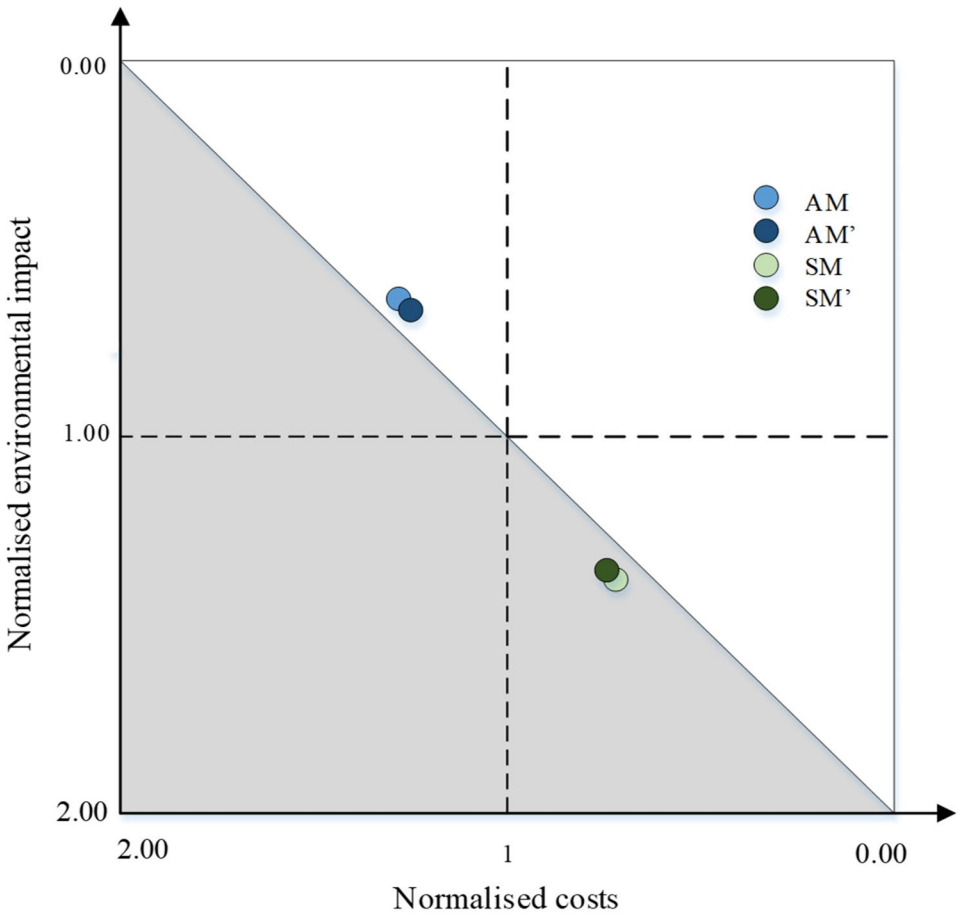

Fig. 13 Eco-efficiency portfolio. (AM, portfolio position of 3D-printed impeller; SM, portfolio position of CNC-machined impeller; AM', revised portfolio position of 3D printed impeller; SM', revised portfolio position of CNC machined impeller)

environmental impact of metal 3D printing is due to a 75.4% reduction of marine eco-toxicity. This shows that metal 3D printing has significant potential to reduce the environmental burden of conventional metal manufacturing. Even though the overall normalised cost of the metal 3D-printed impeller is higher (43.8%) than the CNC-machined impeller, the effect has been offset by the significant reduction of the normalised environmental impact.

The CNC-machined pump impeller has been deemed eco-inefficient due to the significant normalised environmental impact associated with the manufacturing process. This has been significantly contributed by the higher eco-toxicity, which could be due to higher feedstock material wastage in the subtractive process which would end up in landfill or aquatic bodies [16]. The conventional subtractive manufacturing process also uses cutting tools made of carbide or titanium, which possess limited tool life compared to tool-less metal 3D printing. The cutting fluids, which are used to reduce the friction and lower cutting temperature, could also pose significant environmental consequences when disposed to a landfill or aquatic bodies, causing significant eco-toxicity, as evidenced by the ELCA results (Table 18).

Even though the metal 3D-printing process is eco-efficient, it still has a significantly higher cumulative energy demand, which is 40% higher than conventional manufacturing. The metal 3D-printing technology should be further developed to reduce

Table 10 Overall technical figures

Parameter	AM	SM
Surface roughness (shroud R_a) (μm)	2.00	0.923
Surface roughness (vane R_a) (μm)	9.65	0.163
Density (g/cm^3)	7.78	7.94
Dimensional tolerance (mm)	±1.50	±0.25
Tensile strength (MPa)	469	505
Fatigue strength (MPa) at 10^6 cycles	164	201

Table 11 Production plan of impellers

Parameter	AM	SM
Total manufacturing time (hours) per impeller	25.92	6.23
The estimated lifetime of manufacturing equipment (years)	10	10
Annual production output (PO)	101	319

Table 12 LCI of 3D-printed impellers

Stage	Material/process	AM	SM	3D printer	CNC machine
Design	**Energy (kWh)**				
	CAD modelling	0.45	0.45	-	-
Processing	**Transportation (tkm)**				
	Sea	7.33	10.82	21,762.60	17,737.80
	Land	0.02	0.02	54.34	40.00
Manufacturing	**Primary material (kg)**				
	316L stainless steel feedstock	0.343	1.22	-	-
	Wax	0.019	-	-	-
	Polymer binder	0.003	-	-	-
	Material for machines (kg)				
	Steel	-	-	313.50	636.00
	Cast iron	-	-	-	960.00
	Aluminium	-	-	216.03	400.00
	Other plastic	-	-	169.10	2.00
	Copper	-	-	73.15	2.00
	Energy (kWh)				
	3D printer	2.40	4.45	-	-
	Debinder	4.57			
	Sinter	37.97			
	CNC lathe	-	0.58	-	-
	CNC mill	-	2.87	-	-
	Wire EDM	-	0.77	-	-
	Spot welding	-	0.19	-	-
Use	**Energy (kWh)**				
	Use stage	13.2	13.2	-	-

energy consumption, which is particularly significant (84%) in the metal sintering process. Research should be made to investigate the impact of reducing sintering time, sintering temperature, and changing the sintering profile, together with their influence on the technical performance of the metal 3D-printed parts. The trade-off of technical performance to lower the environmental impact of manufacturing could be applied to functional components that do not require high technical performance [17].

Table 13 LCEI values of impellers

Impact category	Unit	Total LCEI		LCEI per Inh	
		AM	SM	AM	SM
GWP	kg CO_2	5.70E + 01	6.52E-01	2.21E-06	2.52E-08
Eutrophication	kg PO_4^{3-} eq	2.34E-02	3.51E-04	9.05E-10	1.36E-11
Land use	Ha. a	2.60E-04	2.78E-06	1.01E-11	1.08E-13
Water use	m^3 H_2O	1.55E-01	1.12E-02	5.99E-09	4.33E-10
CED	MJ	7.48E + 02	2.53E + 00	2.90E-05	9.79E-08
Human toxicity	kg 1,4-DB eq	4.62E + 00	1.15E + 01	1.79E-07	4.44E-07
Freshwater eco-toxicity	kg 1,4-DB eq	1.36E + 00	5.50E + 00	5.27E-08	2.13E-07
Marine eco-toxicity	kg 1,4-DB eq	5.48E + 03	1.12E + 04	2.12E-04	4.33E-04
Terrestrial eco-toxicity	kg 1,4-DB eq	7.09E-02	9.88E-02	2.75E-09	3.82E-09
Acidification	kg SO_2 eq	1.76E-01	1.83E-03	6.80E-09	7.07E-11
ADP	kg Sb eq	2.41E-04	1.52E-06	9.31E-12	5.89E-14
Particulate matter	kg $PM_{2.5}$ eq	1.84E-02	1.96E-04	7.13E-10	7.58E-12
Photochemical smog	kg NMVOC eq	1.92E-01	2.15E-03	7.42E-09	8.31E-11

Table 14 Capital cost and replacement cost breakdown

	Metal 3D printer (AUD)	CNC machine (AUD)
Equipment costs[a,b]	310,000	59,000
Transport cost	1044	1998
Installation cost	-	1000
Extruder[a]	1500	-
Build plate[a]	3500	-
Cutting tools[b]	-	2500
Coolant[c] (20L)	-	600

[a]Objective 3D, Australia and JdLC, Curtin University

[b]Leadwell industries, Taiwan

[c]Rocol Ultracut clear, TW polymers and fluids

The normalised costs of metal 3D printing should also be lowered, which is 78% higher than the normalised cost of conventional manufacturing. The cost of the 3D-printed impeller is higher due to higher material costs associated with innovative metal composite material that allows metal extrusion. The *Desktop Metal* Studio system consists of a printer, debinder, and sintering furnace with a high material footprint and high equipment cost, which is 4.25 times higher than conventional subtractive manufacturing equipment. The excessive costs should be reduced by improvement strategies such as redesigning equipment for integration, which could eliminate duplication, replacing non-critical metallic materials with technically feasible cheaper materials such as composites, eliminating equipment idle time, and using cheaper materials such as polymer matrix compounds.

The inputs may change when these improvement strategies have been implemented for identified hotspots, requiring an update to the LCI. As a result, additional ELCA and LCC would be required to obtain these impellers' revised eco-efficiency portfolio positions. Revised eco-efficiency portfolio positions could be used to determine the comparative benefits of the improvement strategies.

Table 15 Price of the impeller (PI)

	$PV_{total,\ prod.}$ (AUD)	Annuitised cost (AUD)	PO	$LCC_{impeller,\ prod}$ (AUD)	PI (AUD)
AM	554,848	56,324	101	555.53	750
SM	917,357	93,124	319	291.61	394

Table 16 Present values of the pump usage costs

Month	AM impeller		SM impeller	
	Capital cost (AUD)	O&M cost (AUD)	Capital cost (AUD)	O&M cost (AUD)
0	749.96	-	393.70	-
1	-	3.58	-	3.40
2	-	3.57	-	3.38
3	-	3.55	-	3.37
4	-	3.54	-	3.35
5	-	3.52	-	3.34
6	-	3.51	-	3.33
7	-	3.49	-	3.31
8	-	3.48	-	3.30
9	-	3.46	-	3.28
10	-	3.45	-	3.27
11	-	3.43	-	3.26
12	-	3.42	-	3.24
13	-	3.40	-	3.23
14	-	3.39	-	3.22
15	-	3.38	-	3.20
16	-	3.36	-	3.19
17	-	3.35	-	3.18
18	-	3.33	-	3.16
19	-	3.32	-	3.15
20	-	3.30	-	3.14
Total	749.96	68.83	393.70	65.30
$PV_{total,p}$	818.79		459.00	

Table 17 Life cycle cost of pump usage

	$PV_{total,\ P}$ (AUD)	Annuitised cost (AUD)	$LCC_{P,\ SL}$ (AUD)
AM	818.79	537.47	322.48
SM	459.00	301.30	180.78

Table 18 Environmental impacts after normalisation

		AM impeller					SM impeller				
Indicator	W_i	EI	TC	MPC	MfgC	UseC	EI	TC	MPC	MfgC	UseC
GWP	11.44%	2.27E-04	10.46%	3.26%	76.3%	20.1%	1.39E-04	2.91%	33.2%	33.5%	32.9%
Photochemical smog	9.06%	2.31E-04	10.65%	4.71%	75.6%	19.5%	1.19E-04	3.64%	47.6%	26.2%	25.9%
Particulate matter	10.42%	4.27E-05	1.99%	14.8%	67%	18%	4.76E-07	1.20%	70.9%	15.6%	13.4%
Eutrophication	9.51%	1.17E-04	5.39%	5.79%	74.7%	19.2%	2.68E-05	2.50%	27.5%	53.4%	18.9%
Human toxicity	10.08%	1.45E-04	6.67%	8.7%	74.3%	16.8%	3.60E-04	7.52%	23.3%	69.8%	6.74%
Freshwater eco-toxicity	10.08%	8.12E-05	3.74%	15.1%	69.8%	15.1%	1.13E-04	2.36%	19.5%	76.7%	3.8%
Marine eco-toxicity	10.08%	7.97E-04	36.69%	21.6%	65.9%	12.3%	3.22E-03	67.37%	31.7%	62.2%	6.04%
Terrestrial eco-toxicity	10.08%	4.56E-05	2.10%	1.7%	77.3%	21.0%	9.30E-05	1.94%	11.3%	73.5%	15.1%
Land use	8.83%	8.85E-07	0.04%	1.22%	77.4%	21.1%	3.60E-04	0.01%	19.3%	41.1%	39.2%
Acidification potential	8.38%	1.20E-04	5.51%	26.2%	58.8%	14.9%	1.13E-04	5.19%	82.6%	10.1%	7.17%
ADP	9.85%	7.90E-08	0.004%	77.5%	22.4%	0.1%	3.22E-03	0.01%	98.1%	1.85%	0.05%
Water use	10.99%	1.83E-05	0.84%	10.6%	77%	12.2%	9.30E-05	0.56%	15.2%	76.4%	8.29%
CED	11.44%	3.47E-04	15.95%	1.79%	76.2%	22.01%	2.48E-04	4.79%	36.8%	32.6%	30.2%
Total		2.17E-03					4.78E-03				

Table 19 Normalised cost and impact of impellers

Configuration	EIn (inhabitants)	NCn (inhabitants)
AM	2.17E-03	4.58E-03
SM	4.78E-03	2.57E-03

Table 20 Portfolio positions

Impeller	PPe	PPc	PP'e	PP'c
AM	0.6247	1.2816	0.6298	1.2778
SM	1.3753	0.7184	1.3702	0.7222

4 Conclusions, recommendations, and future work

This study has compared the techno-eco-efficiency performance of 316L stainless steel pump impellers made by bound metal deposition metal 3D-printing method and CNC-machining method. The material obtained from metal 3D printing shows a relative density of 97.99% to bulk material density, which is similar to the mean product density of metal injection moulded material. The mean surface roughness of the metal 3D-printed products was slightly higher due to the presence of print lines in the *XY*-direction (+ 1.20 mm) and layer stacking in the *Z*-direction (+ 2.84 mm). Surface treatment methods could improve the surface roughness of these specimens. The tensile test showed ductile properties for the metal 3D-printed specimens with a mean yield strength of 165 MPa, mean tensile strength of 469 MPa, and mean elastic modulus of 191 GPa. These properties are similar to the tensile properties of 316L stainless steel bulk material and metal injection moulded material. The fatigue test of metal 3D-printed specimens indicated a fatigue strength of 164 MPa, which could withstand more than 10^6 fatigue cycles under the fatigue loading of 10 MPa and therefore represents essentially infinite fatigue lifetime under ideal loading conditions. The hydraulic performance curves showed comparatively higher performance than the OEM pump impeller curve. These results showed that the metal 3D-printed specimen is technically feasible for the application of sewage pump considered.

The ELCA of the metal 3D printed pump impellers showed higher environmental impacts for marine eco-toxicity, cumulative energy demand, global warming potential, and photochemical smog. The cumulative energy demand of metal 3D printing was higher compared to CNC machining due to the energy-intensive sintering process (84% of the cumulative energy demand). The life cycle costs of a metal 3D -printed impeller is 1.78 times higher than a conventional subtractive manufactured impeller. The metal 3D-printed pump impeller was found to be eco-efficient than the CNC-machined pump impeller due to having a 54.6% lower normalised environmental impact than the latter. The cumulative energy demand in metal 3D printing was identified as the environmental hotspot due to the energy-intensive sintering process of metal 3D printing. High material costs and equipment costs exist due to the intellectual properties associated with the novel technology. The eco-efficiency of metal 3D-printed pump impellers could be improved by technological strategies by analysing the sintering profile to reduce uneven part shrinkage, improving technical performance and cost reduction of machines by part integration,

replacing non-critical components with cheaper parts, and eliminating equipment idle time.

The metal 3D-printing technology investigated was limited to the bound metal deposition o f 316L stainless steel materials using a *Desktop Metal* Studio printer. In contrast, CNC machining was limited to 316L stainless steel bulk material machining using *Leadwell* CNC lathe machine, *Leadwell V30* vertical milling machine, and *FANUC Robocut* Wire EDM. Furthermore, the results could change with different materials and improved 3D printing and CNC-machining equipment. A new version of the *Desktop Metal* Studio has eliminated the need for a debinder, which would further reduce the manufacturing time, energy consumption, and eliminate the use of chemicals. The benefits of resource minimisation with topology optimisation of the 3D model in 3D printing were not explored as the 3D model was based on the OEM part. The study also did not consider the failure rate of manufactured parts in mass manufacturing as the research mainly focused on the technical feasibility of manufactured impellers. The EE analysis considers a single value of the environmental impact by normalising, weighting, and aggregating the environmental impacts quantified in the ELCA analysis. However, there could be some uncertainties associated with the use of economic and environmental data, which can be addressed in future research using a Monte Carlo simulation.

Future research could conduct a similar techno-eco-efficiency assessment of 3D-printed products using recycled stainless steel feedstock material. Secondly, the surface properties of the metal 3D-printed impellers could be further improved by polishing impeller blade profiles after metal AM could be investigated. Thirdly, a finite element modelling with numerical simulations can be included in the techno-eco-efficiency analysis to optimise the process parameters. These additional tasks can be conducted in the near future to support the adoption of metal 3D-printing technology as a sustainable option in automotive, aerospace, oil and gas, medical, and other industrial applications. Future research should also consider the social implications (e.g., job losses) of the replacement of the conventional subtractive manufacturing supply chain with 3D printing process.

Appendix 1

Table 21 Factors for normalisation and weighing of the environmental impacts [31]

Environment impacts (EIs)	$GDEI_i$	Unit (per inhabitant/y)	Weight (W_i)
Global warming potential (GWP)	28,690	t CO_2 eq	11.44%
Photochemical smog	75	kg NMVOC	9.06%
Particulate matter	45	kg $PM_{2.5}$ eq	10.42%
Eutrophication	19	kg PO_4^{3-} eq	9.51%
Human	3216	kg 1,4-DB eq	10.08%
Terrestrial	88	kg 1,4-DB eq	10.08%
Freshwater	172	kg 1,4-DB eq	10.08%
Marine	12,117,106	kg 1,4-DB eq	10.08%
Land use	26	Ha a	8.83%
Acidification potential	123	kg SO_2 eq	8.38%
Abiotic depletion potential (ADP)	300	kg Sb eq	9.85%
Water use	930	m^3 H_2O	10.99%
Cumulative energy demand (CED)	246900	MJ	11.44%

CO_2 carbon dioxide, *NMVOC* non-methane volatile organic compound, *$PM_{2.5}$* particulate matter, *PO_4^{3-}* phosphate, *DB* dichlorobenzene, *Ha a.*, hectare per year, *SO_2* sulphur dioxide, *Sb* antimony, *H_2O* water, *eq.* equivalent, *MJ* megajoule

Appendix 2

Table 22 PV of the production costs of 3D-printed impeller benchmarked with the production costs of the CNC-machined impeller

	Capital cost		Replacement cost				Manufacturing cost	
Year	3D printer	CNC machine	Extruder	Build plate	Coolant	Cutting tools	AM	SM
0	311044	61998						
1	-	-	2804	0	560.7	2336.4	25,070	102,621.1
2	-	-	4005	0	534.0	2225.1	23,875	97,729.8
3	-	-	3814	3023	508.6	2119.0	22,737	93,071.6
4	-	-	3632	0	484.3	2018.0	21,654	88,635.5
5	-	-	3459	0	461.2	1921.8	20,621	84,410.8
6	-	-	3294	2611	439.3	1830.2	19,639	80,387.5
7	-	-	3137	0	418.3	1743.0	18,703	76,556.0
8	-	-	2988	0	398.4	1659.9	17,811	72,907.0
9	-	-	2845	2255	379.4	1580.8	16,962	69,432.0
10	-	-	2710	0	361.3	1505.5	16,154	66,122.6
Total	14949	64224	32,690	7889	4545.6	18,939.9	203,226	831,873.9

All costs are in AUD

Acknowledgements The authors are grateful for the technical support provided by the staff of Curtin University.

Author contribution All authors contributed to conceptualisation and methodology. Analysis, investigation, data curation, writing - original draft, and visualisation were performed by H.J. All authors contributed to writing - review and editing. All authors read and approved the final manuscript.

Funding Open Access funding enabled and organized by CAUL and its Member Institutions. The authors would like to gratefully acknowledge the financial support provided by the Sustainable Engineering Group scholarship of Curtin University.

Data availability The research data and material will be made available at Curtin Research Data Collection.

Declarations

Ethics approval The ethics approval for this research work was obtained from Curtin University under approval number HRE2020-0203.

Competing interests The authors declare no competing interests.

References

1. World Bank (2019) National accounts data. https://data.worldbank.org/indicator/NV.IND.MANF.ZS?end=2020&start=2012. Accessed 14 Aug 2020
2. International Energy Agency, Key world energy statistics (2020) Available: https://iea.blob.core.windows.net/assets/1b7781df-5c93-492a-acd6-01fc90388b0f/Key_World_Energy_Statistics_2020.pdf. Accessed 19 Nov 2020
3. Intergovernmental Panel on Climate Change, Climate Change (2021) the physical science basis. Contribution of Working Group I to the Sixth Assessment Report of the Intergovernmental Panel on Climate Change. Available: https://www.ipcc.ch/report/ar6/wg1/downloads/report/IPCC_AR6_WGI_Full_Report.pdf. Accessed 20 Mar 2021
4. Huang R et al (2016) Energy and emissions saving potential of additive manufacturing: the case of lightweight aircraft components. J Clean Prod 135(3):1559–1570. https://doi.org/10.1016/j.jclepro.2015.04.109
5. Peng T, Kellens K, Tang R, Chen C, Chen G (2018) Sustainability of additive manufacturing: an overview on its energy demand and environmental impact. Add Manuf 21(5):694–704. https://doi.org/10.1016/j.addma.2018.04.022
6. Australian Renewable Energy Policy (2020) Renewable energy in the Australian mining sector. Available: https://arena.gov.au/knowledge-bank/renewable-energy-australian-mining-sector/. Accessed 15 Mar 2021
7. Peng S, Li T, Wang X, Dong M (2017) Toward a sustainable impeller production: environmental impact comparison of different impeller manufacturing methods. J Ind Ecol 21(S1):S216–S229. https://doi.org/10.1111/jiec.12628
8. Ingarao G, Priarone PC, Deng Y, Paraskevas D (2018) Environmental modelling of aluminium based components manufacturing

routes: additive manufacturing versus machining versus forming. J Clean Prod 176(6):261–275. https://doi.org/10.1016/j.jclepro.2017.12.115
9. Priarone PC, Ingarao G (2017) Towards criteria for sustainable process selection: on the modelling of pure subtractive versus additive/subtractive integrated manufacturing approaches. J Clean Prod 144(16):57–68. https://doi.org/10.1016/j.jclepro.2016.12.165
10. Fatimah YA, Biswas W, Mazhar I, Islam MN (2013) Sustainable manufacturing for Indonesian small- and medium-sized enterprises (SMEs): the case of remanufactured alternators. J Remanuf 3(1):6. https://doi.org/10.1186/2210-4690-3-6
11. Jayal AD, Badurdeen F, Dillon OW, Jawahir IS (2010) Sustainable manufacturing: modeling and optimization challenges at the product, process and system levels. CIRP J Manuf Sci Technol 2(3):144–152. https://doi.org/10.1016/j.cirpj.2010.03.006
12. Serres N, Tidu D, Sankare S, Hlawka F (2011) Environmental comparison of MESO-CLAD® process and conventional machining implementing life cycle assessment. J Clean Prod 19(9):1117–1124. https://doi.org/10.1016/j.jclepro.2010.12.010
13. Galati M, Minetola P (2019) Analysis of density, roughness, and accuracy of the atomic diffusion additive manufacturing (ADAM) process for metal parts. Materials 12(24):4122. https://doi.org/10.3390/ma12244122
14. Le VT, Paris H (2018) A life cycle assessment-based approach for evaluating the influence of total build height and batch size on the environmental performance of electron beam melting. Int J Adv Manuf Technol 98(1):275–288. https://doi.org/10.1007/s00170-018-2264-7
15. Tang Y, Mak K, Zhao YF (2016) A framework to reduce product environmental impact through design optimization for additive manufacturing. J Clean Prod 137(15):1560–1572. https://doi.org/10.1016/j.jclepro.2016.06.037
16. Ma J, Harstvedt JD, Dunaway D, Bian L, Jaradat R (2018) An exploratory investigation of Additively Manufactured Product life cycle sustainability assessment. J Clean Prod 192(29):55–70. https://doi.org/10.1016/j.jclepro.2018.04.249
17. Thompson Y, Gonzalez-Gutierrez J, Kukla C, Felfer P (2019) Fused filament fabrication, debinding and sintering as a low cost additive manufacturing method of 316L stainless steel. Addit Manuf 30:100861. https://doi.org/10.1016/j.addma.2019.100861
18. Le VT, Paris H, Mandil G (2017) Environmental impact assessment of an innovative strategy based on an additive and subtractive manufacturing combination. J Clean Prod 164:508–523. https://doi.org/10.1016/j.jclepro.2017.06.204
19. Faludi J, Baumers M, Maskery I, Hague R (2017) Environmental Impacts of selective laser melting: do printer, powder, or power dominate? J Ind Ecol 21(S1):S144–S156. https://doi.org/10.1111/jiec.12528
20. Baumers M, Tuck C, Hague R, Ashcroft I, Wildman R (2010) A comparative study of metallic additive manufacturing power consumption. Solid Freeform Fabric Symp 2009:278–288. https://doi.org/10.26153/tsw/15198
21. Lengauer W et al (2019) Fabrication and properties of extrusion-based 3D-printed hardmetal and cermet components. Int J Refract Metal Hard Mater 82:141–149. https://doi.org/10.1016/j.ijrmhm.2019.04.011
22. Masood SH, Song WQ (2004) Development of new metal/polymer materials for rapid tooling using Fused deposition modelling. Mater Des 25(7):587–594. https://doi.org/10.1016/j.matdes.2004.02.009
23. Desktop Metal (2020) Studio system overview. https://www.desktopmetal.com/products/studio. Accessed 15 Jul 2020
24. Markforged (2021) Metal X 3D printer. https://markforged.com/3d-printers/metal-x. Accessed 15 Mar 2021
25. Jiang D, Ning F (2021) Additive manufacturing of 316L stainless steel by a printing-debinding-sintering method: effects of microstructure on fatigue property. J Manuf Sci Eng 143(9):091007. https://doi.org/10.1115/1.4050190
26. Sadaf M, Bragaglia M, Nanni F (2021) A simple route for additive manufacturing of 316L stainless steel via Fused Filament Fabrication. J Manuf Process 67:141–150. https://doi.org/10.1016/j.jmapro.2021.04.055
27. Peng T, Wang Y, Zhu Y, Yang Y, Yang Y, Tang R (2020) Life cycle assessment of selective-laser-melting-produced hydraulic valve body with integrated design and manufacturing optimization: a cradle-to-gate study. Additive Manuf 36:101530. https://doi.org/10.1016/j.addma.2020.101530
28. Lindemann C, Jahnke U, Moi M, Koch R (2012) Analyzing product lifecycle costs for a better understanding of cost drivers in additive manufacturing. 23th Ann Int Solid Freeform Fabric Symp An Additive Manuf Conf. Austin Texas USA 6th-8th August. https://doi.org/10.26153/tsw/15341
29. Bengtsson M, Kurdve M (2016) Machining equipment life cycle costing model with dynamic maintenance cost. Procedia CIRP 48:102–107. https://doi.org/10.1016/j.procir.2016.03.110
30. Watson A, Belding J, Ellis BD (2020) Characterization of 17–4 PH processed via bound metal deposition (BMD). TMS 2020 149th Ann Meet Exhibit Suppl Proc. Springer, 205–216. https://doi.org/10.1007/978-3-030-36296-6_19
31. Jayawardane H, Davies IJ, Leadbeater G, John M, Biswas WK (2021) 'Techno-eco-efficiency' performance of 3D printed impellers: an application of life cycle assessment. Int J Sustain Manuf 5(1):44–80. https://doi.org/10.1504/ijsm.2021.116871
32. Grundfos (2020) Grundfos Unilift KP250. https://product-selection.grundfos.com/products/unilift-kp/unilift-kp-250-a-1-012H1800?tab=variant-specifications. Accessed 18 Nov 2020
33. Pertuz AD, Díaz-Cardona S, González-Estrada OA (2020) Static and fatigue behaviour of continuous fibre reinforced thermoplastic composites manufactured by fused deposition modelling technique. Int J Fatigue 130(19):105275. https://doi.org/10.1016/j.ijfatigue.2019.105275
34. Rotodynamic pumps — Hydraulic performance acceptance tests — Grades 1, 2 and 3 (2012) International Organization for Standardization
35. Environmental management — Life cycle assessment — Principles and framework (2006) International Organisation for Standardization
36. Arceo A, Biswas WK, John M (2019) Eco-efficiency improvement of Western Australian remote area power supply. J Clean Prod 230(1):820–834. https://doi.org/10.1016/j.jclepro.2019.05.106
37. Life cycle costing - An application guide AS/NZS 4536–1999 (1999) Standards Australia/ Standards New Zealand
38. PayScale (2020) 3D designer salary in Australia. https://www.payscale.com/research/AU/Job=3D_Artist/Salary. Accessed 12 Feb 2020
39. Australian Government (2015) Rail, road, and sea freight costs. https://www.bitre.gov.au/sites/default/files/is_090.pdf. Accessed 13 Mar 2020
40. Canstar Blue (2020) Perth electricity prices. https://www.canstarblue.com.au/electricity/perth-electricity-prices/. Accessed 24 Apr 2020
41. Australian Bureau of Statistics (2018) Employee earnings and hours, Australia. [Online]. Available: https://www.abs.gov.au/ausstats/abs@.nsf/0/27641437D6780D1FCA2568A9001393DF?Opendocument. Accessed 19 Aug 2020
42. Trading Economics. Australia inflation rate (2020) https://tradingeconomics.com/australia/inflation-cpi. Accessed 5 Apr 2020
43. Department of the Prime Minister and the Cabinet (2016) Cost benefit analysis - guidance note. [Online]. Available: https://www.

pmc.gov.au/sites/default/files/publications/cosst-benefit-analysis.docx. Accessed 10 Nov 2020
44. Plumbing and Mechanical. Pumpin material markup (2000) https://www.pmmag.com/articles/102066-material-markup. Accessed 15 Mar 2020
45. Department of the Environment and Energy (2019) Australian energy update 2019
46. Bengtson J, Howard N (2010) A life cycle impact assessment method for use in Australia—classification, characterisation and research needs. Australia: Edge Environ Pty Ltd
47. Australian Bureau of Statistics (2020) 1345.0 - key economic indicators. [Online]. Available: https://www.abs.gov.au/ausstats/abs@.nsf/productsbytopic/F5BDED213BC207B6CA2579FB0008E577?OpenDocument. Accessed 15 Aug 2020
48. Saling P, Kicherer A, Dittrich-Krämer B et al (2002) Eco-efficiency analysis by basf: the method. Int J Life Cycle Assess 7(4):203–218. https://doi.org/10.1007/BF02978875
49. Cheng K, Shao Y, Bodenhorst R, Jadva M (2017) Modeling and simulation of material removal rates and profile accuracy control in abrasive flow machining of the integrally bladed rotor blade and experimental perspectives. J Manuf Sci Eng 139(12). https://doi.org/10.1115/1.4038027
50. Shao Y, Adetoro OB, Cheng K (2021) Development of multiscale multiphysics-based modelling and simulations with the application to precision machining of aerofoil structures. Eng Comput 38(3):1330–1349. https://doi.org/10.1108/EC-10-2019-0473
51. Gong H, Snelling D, Kardel K, Carrano A (2019) Comparison of stainless steel 316L parts made by FDM- and SLM-based additive manufacturing processes. JOM 71(3):880–885. https://doi.org/10.1007/s11837-018-3207-3
52. Optimim (2021) MIM 316L. https://www.optimim.com/metal-injection-molding-mim/material-options/stainless-steel/mim-316l. Accessed 14 Jan 2021
53. Cheah K, Lee L, Winoto S, Zhao Z (2007) Numerical flow simulation in a centrifugal pump at design and off-design conditions. Int J Rotating Mach 2007. https://doi.org/10.1155/2007/83641
54. Wang Z, Yang S, Huang Y, Fan C, Peng Z, Gao Z (2021) Microstructure and fatigue damage of 316L stainless steel manufactured by selective laser melting (SLM). Materials 14(24):7544. https://doi.org/10.3390/ma14247544
55. West Marine (2019) Impeller replacement. https://www.westmarine.com/WestAdvisor/Impeller-Replacement-101. Accessed 10 Mar 2020
56. Strongman Pumps (2020) The Difference between sewage, sump, drainage & more. https://www.strongmanpumps.com.au/difference-sewage-sump-drainage-pumps/. Accessed 15 May 2020
57. Santonen T, Stockmann-Juvala H, Zitting A (2010) Review on toxicity of stainless steel, Työterveyslaitos, 9522610399. [Online]. Available: https://core.ac.uk/download/pdf/84322713.pdf. Accessed 12 Nov 2020